Table 4. Summary of conditions for Co SX by Cyanex 272 from NMC LIBs real or simulated leachates and other Co and Ni-bearing solutions available in the literature. If not otherwise stated, when more than one stage is indicated, counter-current extraction must be intended.

Solvent Composition	Feed					Number of stages	Extraction						Source
	Leachate	Composition(g/L)					θ	pH$_{eq}$	Efficiency				
		Mn	Co	Ni	Li				Mn	Co	Ni	Li	
Cyanex 272 0.8 M Exxsol D80	Synthetic	0.1	16.2	2.0	2.2	3	2.5	5.4 4.9 3.7	100%	99.8%	<0%* *affected by the operation control	11.5%	[14]
Cyanex 272 0.6-0.8 M Isopar L	LIBs leachate HCl	0.1	8.3	1.9	0.9	1-3	<0.9	<5.0	100%	<98%	<5%	NA	[70]
Cyanex 272 0.13 M Kerosene	Purified Cu raffinate (SO$_4^{2-}$)	/	1.7	16.4	/	2	0.9	NA (60% Na-Cyanex 272)	/	99.9%	0.2%	/	[71]
Cyanex 272 0.2 M Kerosene	Synthetic (SO$_4^{2-}$)	/	1.8	16.8	/	2	0.66	NA (50% Na-Cyanex 272)	/	99.9%	<1%	/	[72]
Cyanex 272 0.4 M Kerosene	LIB leachate H$_2$SO$_4$	/	13.8	15.0	2.0	2	2	5.5-6.0	/	99.9%	1%	1%	[82]
Cyanex 272 0.64 M Kerosene	LIB leachate H$_2$SO$_4$	/	10.0	/	/	2	1	5.0 (50% Na-Cyanex 272)	NA	>99%* *from McT diagram	NA	NA	[83]

11

3 Theory

3.1 Solvent Extraction

Liquid-liquid extraction, traditionally known as solvent extraction, is a process which involves the distribution of a solute between two not completely mutually miscible liquid phases of different densities. The difference between the solute-solvent interaction in the two phases is the driving force for the solute distribution. The extraction process can be distinguished as non-reactive, if only the solubility of the solute determines its partition, or reactive, if the solutes react with another species (extractant) to form a compound with new distribution features. The latter is commonly employed in hydrometallurgy [84–86]. Most of the solvent extraction systems used for hydrometallurgical purposes comprise an aqueous heavy phase and an organic light phase. The aqueous phase is usually an electrolyte solution containing metal ions, whereas the organic phase is normally composed of an extractant, a diluent and eventually other components (e.g., phase modifier, antioxidants). As detailed in the following sections, the extraction of metal ions is affected by several equilibrium reactions which can take place in the aqueous phase, in the organic phase and at the interface [84–86].

3.2 Solution Chemistry

In solutions containing metal ions, various metal species can exist in a dynamic equilibrium, and their relative abundance depends on temperature, pH, ionic strength, and redox potential. The electrolyte concentration in a solution can be measured by its ionic strength:

$$I = \frac{1}{2} \sum_i^n c_i z_i^2 \tag{1}$$

Where c_i and z_i are the ion concentration [mol/L][1] and charge, respectively [84,87]. As the ionic strength of a solution increases, interactions between the dissolved metal and the electrolyte ions increase and deviations from ideal behaviour are expected. The chemical activity (a_i) is used to express the effective concentration of a species in such a solution. The activity can be expressed as:

$$a_i = \gamma_i \frac{c_i}{c_0} \tag{2}$$

Where c_i and c_0 are the actual concentration [mol/L][1] of the species i in the solution and the standard state ($c_0 = 1.0$ M), respectively. γ_i are the activity coefficients and account for deviations from ideal behaviour. The activity coefficients of aqueous species can be computed using models which are accurate in different ranges of ionic strength (e.g., Debye-Hückel, SIT, Pitzer) [84,88,89].

The formation of different metal-ligand complexes in solution can be described by a series of stepwise reactions. For mononuclear complexes, the successive complexation reactions can be expressed as follows:

---

[1] Ionic strength and activities are here defined using mol/L for coherency with the rest of the text. The definition of these quantities is however commonly given in terms of molality [mol/Kg] to remove the dependency on the temperature.
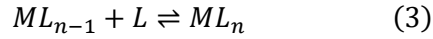
$$ML_{n-1} + L \rightleftharpoons ML_n \qquad (3) \qquad\qquad K_n = \frac{\{ML_n\}}{\{ML_{n-1}\}\{L\}} \qquad (4)$$

Where M indicates the metal, L the ligand, K_n is the equilibrium constant for the stepwise reaction. The curly brackets indicate the activity of a certain species and charges are omitted for simplicity. The overall reaction for the formation of multiligand mononuclear complexes can be generalized as:

$$M + nL \rightleftharpoons ML_n \qquad (5) \qquad\qquad \beta_n = \frac{\{ML_n\}}{\{M\}\{L\}^n} = \prod_i^n K_i \qquad (6)$$

Where β_n is the cumulative stability constant [84].

3.3 Quantitative evaluation of solvent extraction systems

The efficiency with which a metal species M is extracted by an SX system is quantitatively expressed with the distribution ratio (D_M). D_M is defined as the ratio of the total analytical concentration of the element in the organic phase to its total analytical concentration in the aqueous phase, usually measured at equilibrium [84]:

$$D_M = \frac{\overline{[M]}}{[M]} \qquad (7)$$

Where the overbar indicates that a certain species is in the organic phase. It is important to notice that, differently from the stability constants previously derived, the distribution ratio is defined in terms of concentrations. From the distribution ratio, the extraction efficiency ($\%E_M$) can be computed as:

$$\%E_M = 100 \cdot \frac{D_M}{D_M + 1/\theta} \qquad (8)$$

Where θ is the ratio of the organic and aqueous phase volume [84]. The selectivity of an extraction system for a solute M compared to a solute N is expressed by the separation factor (SF):

$$SF_{M/N} = \frac{D_M}{D_N} \qquad (9)$$

By convention the solutes M and N are chosen so that $SF_{M/N}$ is >1 [90]. The relative purity of a target species ($P_{R,M}$) in a specific stream of a solvent extraction system can be computed as:

$$P_{R,M} = 100 \cdot \frac{w_M}{\sum_i w_i} \qquad (10)$$

Where w indicates the mass or the moles of the metal in the product, and i is an index that refers to all the considered metals. It is common practice in hydrometallurgy to report the relative purity in terms of mass.
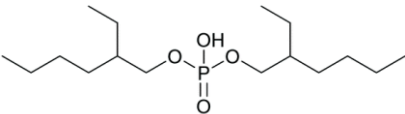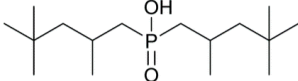
3.4 Extraction Mechanism of Acidic Extractants

The most relevant extractants for metal complexes are [84]:

- Chelating/acidic extractants
- Adduct/neutral extractants
- Anionic extractants

The extractants used in this work (Table 5), are acidic extractants, therefore only the extraction mechanism related to those is discussed.

Table 5. Extractants for Mn, Co and Ni SX for LIBs. pKa values are reported for water/extractant system according to [91,92].[2]

Extractant	Molecule	pKa	Applications
D2EHPA		2.79	Mn/Co separation
			Ni/Li separation
Cyanex 272		3.73	Co/Ni separation
			Co, Mn extraction
			Ni/Li separation

The simplified overall extraction reaction for a metal *M* by an acidic extractant can be generalized as:

$$M^{\nu+} + \nu\overline{HA} \rightleftharpoons \overline{MA_\nu} + \nu H^+ \qquad (11)$$

Where $M^{\nu+}$ is the metal species to be extracted, and *HA* is the undissociated extractant. The equilibria involved in the extraction process are reported in Figure 3. The equilibrium constants for such reactions are reported in Equations (12-15).

$$K_D = \frac{\overline{\{HA\}}}{\{HA\}} \qquad (12) \qquad\qquad K_a = \frac{\{H^+\}\{A^-\}}{\{HA\}} \qquad (13)$$

$$\beta_n = \frac{\{MA_n^{\nu-n}\}}{\{M^{\nu+}\}\{A^-\}^n} \qquad (14) \qquad\qquad \lambda_\nu = \frac{\overline{\{MA_\nu\}}}{\{MA_\nu\}} \qquad (15)$$

---

[2] The pKa value depends on the media in which it is determined, and its accuracy is a function of the methods used for its determination. An overview of the pKa available in the literature for such extractants and their reliability is given in [122].
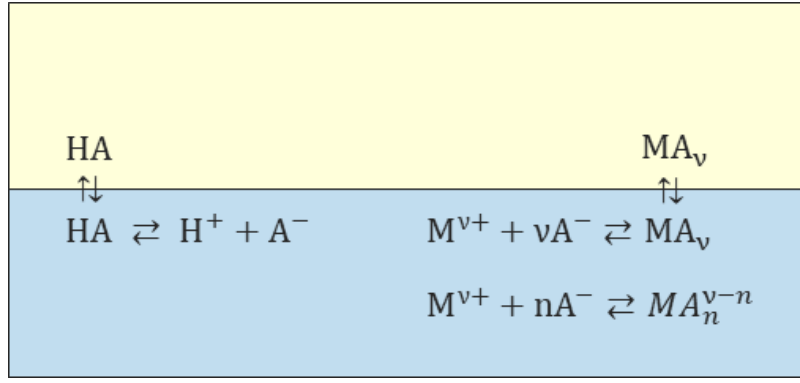
Figure 3. Simplified representation of the equilibria involved in the extraction of a metal (M) as a coordinatively saturated complex (MAv) by an acidic extractant (HA). The organic phase is represented in yellow, while the aqueous phase is in blue. The formation extractant adducts in the solvent and side reactions in the aqueous phase are omitted for simplicity.

Considering all the species containing *M* in the system and conveniently substituting Equations (2, 14, 15), the following expression for the distribution ratio can be written:

$$D_M = \frac{[\overline{MA_v}]}{\sum_{n=0}^{m}[MA_n^{v-n}]} = \frac{\lambda_v \beta_v \gamma_{MA_v}^{-1}\{A^-\}^v}{\sum \beta_n \gamma_{MA_n}^{-1}\{A^-\}^n} \tag{16}$$

The mass balance on *A⁻* for such a system can be written as:

$$\overline{V}[\overline{HA_0}] = \overline{V}[\overline{HA}] + V([HA] + [A^-]) \tag{17}$$

Where *[HA₀]* is the initial concentration of extractant. By expressing the mass balance in terms of activities and substituting Equations (12,13), the following expression for {*A⁻*} can be derived:

$$\{A^-\} = \frac{\{\overline{HA_0}\}}{\frac{K_D}{K_a \gamma_{HA}}\{H^+\} + \frac{1}{\theta}\left(\frac{\{H^+\}}{K_a \gamma_{HA}} + \frac{1}{\gamma_{A^-}}\right)} \cdot \frac{1}{\gamma_{\overline{HA_0}}} \tag{18}$$

From Equation (18), it can be seen that {*A⁻*} is a function of the initial activity of the extractant, the proton activity in the solution at equilibrium (pH) and the volume ratio of the phases (θ). Consequently, also the distribution ratio that, according to Equation (16), depends on {*A⁻*}, will be a function of such parameters. Moreover, as the equilibrium constants are a function of pressure and temperature, D_M will also depend on them.

From Equations (11,18), it is evident that the pH plays a relevant role on the equilibrium of the extraction and that during the extraction protons are released proportionally to the quantity of metal extracted. Higher variations in the equilibrium pH are therefore expected for systems in which higher quantities of metals are extracted. However, when the acidity of the aqueous solution increases, the extraction is hindered. Accurate control of the equilibrium pH becomes then important to achieve the desired selectivity when using acidic extractants [86]. The addition of a base (e.g., NaOH) to the two phases during mixing or to the solvent before extraction (pre-neutralization or saponification) are the two methods commonly used for such operation [84]. When NaOH is used, the saponification reaction can be written as:

$$NaOH + \overline{HA} \rightleftharpoons \overline{NaA} + H_2O \tag{19}$$

Depending on the fraction of extractant (*HA*) that is converted to its sodium salt (*NaA*), the degree of saponification (*N*) can be computed as:

$$N(\%) = 100 \cdot \frac{[\overline{NaA}]}{[\overline{HA}]} \qquad (20)$$

3.5 Phase behaviour in metals extraction systems

To achieve high solubility in low-polarity diluents, the extractants used for metal extraction are normally composed of a polar head group and one or more branched hydrocarbon chains, showing an amphiphilic surfactant-like molecular structure. When dissolved in non-polar diluents (e.g., alkanes, simple aromatics), acidic extractants such as organophosphorus acids are known to self-associate to form dimers [86]. However, the level of aggregation can be drastically changed when water, or a water-containing solution (e.g., NaOH, NH$_3$), is added to the solvent, such as in the saponification process (Equation 19). In specific conditions, the increased surface activity of the surfactants will promote the solubilization of water and hydrocarbons in the same thermodynamically stable solution (microemulsion). Formation of lyotropic liquid crystalline phases might also occur [93,94].

In surfactant chemistry, the phase behavior of a water-surfactant-oil system is commonly represented in ternary phase diagrams [95]. Such representation can also be used to describe solvent extraction systems. Specifically, the phase behavior of pre-neutralized solvents can be described by a pseudo-ternary system composed of base-extractant-diluent. Its knowledge, joint to considerations about the solvent's water content and viscosity, and batch SX tests can provide guidelines for selecting suitable saponification conditions (e.g., base, base concentration, temperature) [93].

3.6 Development of SX processes

An example of an industrial solvent extraction process flowsheet is shown in Figure 4. The essential operations in a solvent extraction circuit are extraction and stripping. Depending on the requirements associated with the purity of the final product and on the selectivity of the extraction operation, a scrubbing step might be added to purify the extract [84,86]. Conditioning of the solvent after stripping might be needed, depending on the nature of the extractant and the solvent composition (e.g., saponification). The regenerated solvent is recirculated in the extraction stage until its performances degrade. To reduce the overall cost of the process and minimize waste production, internal recirculation of different output streams is foreseen. For instance, the stripping raffinate might be partly recirculated as scrubbing solution and the scrubbing raffinate could be recovered by mixing with the feed or leaching solution.
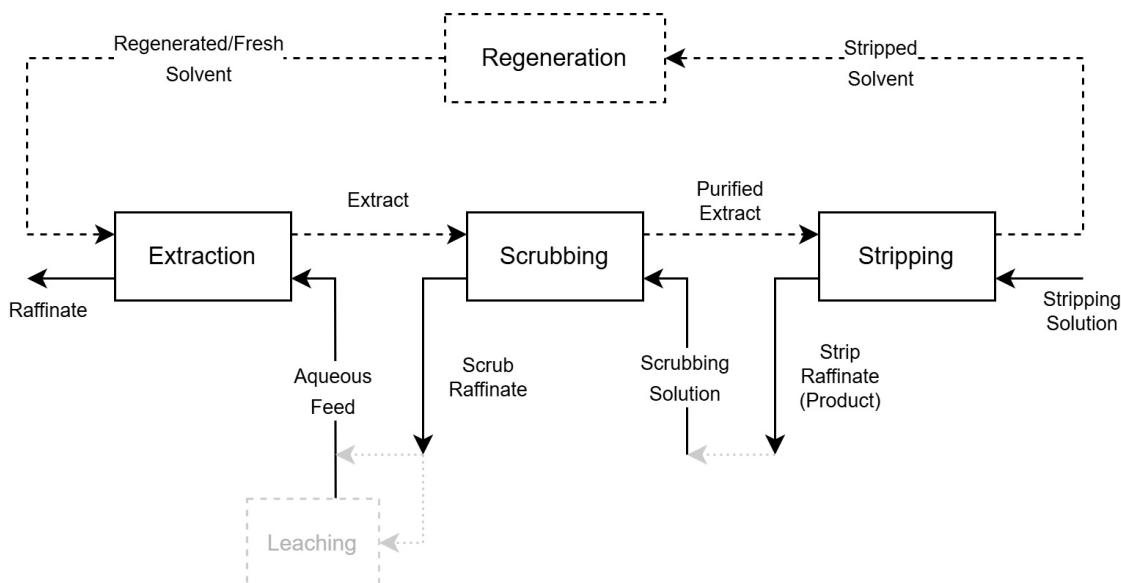
Figure 4. Example of industrial solvent extraction flow sheet. Solid lines: aqueous flows; dashed lines: organic flows; grey lines: hypothetical recirculation.

As explained in section 3.2, composition, pH, redox potential, and ionic strength affect the dynamic equilibrium of the different species existing in the aqueous phase. These variables are directly related to the conditions in which the metals are leached and to all the operations carried out on the solution upstream of solvent extraction. Knowledge of these parameters, joint with information on the physical properties of the phases (e.g., density, viscosity, interfacial tension etc.), is fundamental for the development of a solvent extraction process [84,86]. Batch experiments are initially performed to select a suitable extraction system and to define physical and chemical conditions for its application. The selection of extractant, diluent and eventually a phase modifier is the first step. Parameters such as extractant concentration, pH, kinetics, temperature and phase ratio are investigated. Extractants with fast kinetics are preferred, if available, as they allow for a higher production capacity. Moreover, system's properties, such as phase separation, solvent losses, chemical stability and, if needed, radiolitic stability are also tested.

Normally, satisfactory extraction and separation cannot be achieved in single-stage extractions and multi-stage extraction is implemented at the industrial level. Among the available alternatives, counter-current systems (Figure 5) are normally used as they minimize solvent consumption [84,86]. The number of extraction stages can be determined using e.g. the McCabe-Thiele methodology (Section 3.6.1). Different equipment (e.g., mixer settlers, columns, centrifugal contactors) can be selected for the scale-up of solvent extraction processes, and many designs are available for each of them [96]. After batch experiments, pilot tests are usually carried out for further optimization of the process before the final scale-up. However, different strategies might be adopted depending on the novelty of the process, the economical availability and time [84].
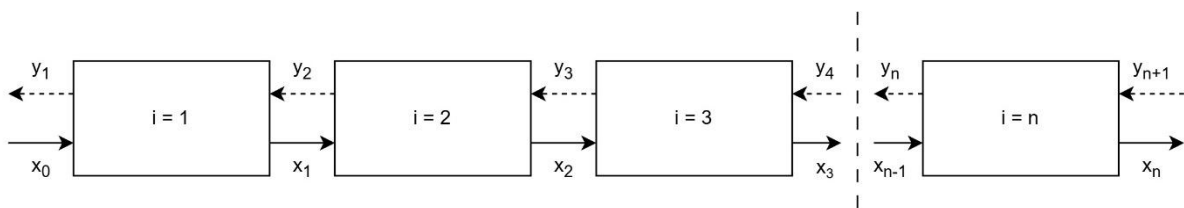
Figure 5. Schematic of a counter-current solvent extraction system. x indicates the heavy phase flow; y indicates the light phase.

3.6.1 McCabe-Thiele Diagrams

The number of counter-current stages needed to achieve the desired efficiency with a specific extraction system can be defined by using graphical methods such as the McCabe-Thiele diagram [84,86]. In this method, an extraction curve and an operating line are plotted and used to graphically solve the mass balance for each stage of the extraction cascade. The operating line is obtained by solving the mass balance of the cascade (Figure 5) and is usually a straight line of slope θ^{-1}. The coordinates of such a line are defined by the feed concentration of the target solute (x_0), the phase ratio (θ) and the targeted solute content in the raffinate after extraction (x_n). The extraction curve is instead a plot of equilibrium concentrations of the solute in the aqueous and organic phases and must be experimentally determined. To do so, the solvent and the aqueous phase are usually contacted at different θ and fixed pH and temperature. The number of stages is finally determined by drawing vertical and horizontal lines as in Figure 6. McCabe-Thiele diagrams for scrubbing and stripping can also be determined with similar methodology, except that the concentration of the metal in the organic phase is in this case plotted on the x-axis [84,86]. One of the major hypotheses behind the determination of extraction stages with McCabe-Thiele diagrams is that equilibrium is reached at every extraction stage, nevertheless, this is rarely the case when multi-stage continuous solvent extraction systems are scaled up. "Shrinking" of the equilibrium curve might be observed in presence of cascade inefficiencies and a higher number of stages might be needed for achieving the desired efficiency [84].
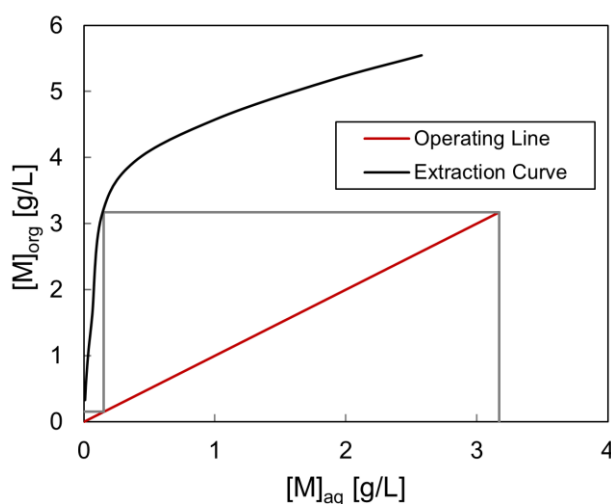

Figure 6. McCabe-Thiele diagram for the extraction of a generic metal M.

3.7 Principles of Evaporative Crystallization

Crystallization is a chemical operation which involves the formation of a solid with a crystalline structure from a liquid phase. The driving force and prerequisite for the nucleation and growth of crystals in solution is supersaturation. For a generic reaction between a metal ion and a counter-ion, the crystallization reaction and its equilibrium constant (solubility product, K_{sp}) can be written as:

$$aM + bL \rightleftarrows M_a L_b(s) \qquad (21) \qquad\qquad K_{sp} = \{M\}^a \{L\}^b \qquad (22)$$

Supersaturation of the solution is reached when the products of the activities of the ions in the aqueous solution is higher than the solubility product. In a binary water-salt system, supersaturation can be achieved by evaporation of the solvent (Evaporative Crystallization - EC).

4 Materials and methods

4.1 Feed solutions

Two different feed solutions produced from NMC111 and NMC9.5.5 spent lithium-ion batteries were used in this work. NMC111 EV battery modules were provided by Volvo Cars AB (Sweden) and their dismantling and discharging was performed by STENA Recycling AB (Sweden). Crushing and mechanical separation were carried out by Akkuser Oy (Finland). The NMC9.5.5 modules were provided by Morrow (Norway) and dismantled, discharged, crushed and mechanically separated by Orano (France). In both cases the produced black mass was leached using conditions developed by Aalto University (Finland, 2 M H_2SO_4, S/L = 200 g/L, T = 50°C). Both leaching and impurities (Cu, Fe, Al) removal was carried out by Metso (Finland). Cu was removed from the PLS by precipitation of CuS through the addition of a stoichiometric amount of gaseous H_2S at 50°C. Al and Fe were selectively precipitated by addition of NaOH and H_2O_2 at temperatures between 50 and 80°C. The NMC111 PLS was used as received in Paper I. During the treatment of the NMC9.5.5 PLS, an anionic and a cationic flocculant were added to ease the filtration in the impurities removal stage. The purified PLS was further treated to remove Mn in three counter-current stages ([D2EHPA] = 0.3 M in Isopar L, pH = 3.5 ± 0.1, θ = 1) and was used in Manuscript II. The compositions of the feeds are reported in Section 5.

4.2 Chemicals

Bis(2-ethylexyl) phosphoric acid (D2EHPA, 97%, Sigma Aldrich, Germany), Bis(2,4,4-trimethylpentyl) phosphinic acid (Cyanex 272, 85-95% BTMPPA, Cytec, USA) and Isopar L (Exxon Mobil, USA) were used without further purification to prepare the solvents used in this work. The BTMPPA content in Cyanex 272 was measured to be 91.3 ± 0.8 wt% (2.90 ± 0.01 M) by potentiometric titration (Appendix B). NaOH pellets (>99%, EMSURE or >98%, Sigma Aldrich, Germany) were dissolved in MQ-water to prepare the solutions used for pH control. H_2SO_4 (95-98%, Sigma Aldrich, Germany) was either used as such for pH adjustment or diluted in Milli-Q water (resistivity = 18 MΩ·cm) to prepare acidic stripping solutions. $MnSO_4 \cdot H_2O$ (>99%, Sigma Aldrich, Germany) was dissolved in Milli-Q water to prepare the phases used for scrubbing in Paper I. HNO_3 (65 or 69% suprapur, Merck, Germany) was used after dilution to prepare the samples for ICP analysis. Standard solution for ICP analysis were prepared starting from elemental stocks (1000 ppm, Inorganic Ventures).

4.3 Experimental procedures

4.3.1 Solvent Extraction

Batch SX experiments were carried out in 100 mL PP vessels contacting a total volume of about 30 mL. pH adjustment was performed by addition of 10 M NaOH or concentrated H_2SO_4 solutions. Sampling of the heavier phase was performed after satisfactory phase separation was visually observed. When no direct pH control was required, experiments were carried out in glass vials (3.5 mL) using a shaking machine (IKA-Vibrax, Germany). Samples were centrifuged at 5000 rpm for 5 min to guarantee satisfactory phase separation. When possible, back extraction of the loaded organic with 5 M H_2SO_4 at A:O = 5 was performed and the raffinates were analysed to measure the concentration of metals in the solvent and validate the mass balance.

Pseudo counter-current (Pseudo-cc) simulations were carried out following the schemes reported in Figure 7. To simulate each stage, the aqueous and organic phase were equilibrated in a 100 mL PP vessel. Phase disengagement was achieved in a separation funnel. The system was assumed to approach steady state when the concentration of metals in the outlet streams remained constant in three consecutive cycles. Differently from a pseudo counter-current simulation, equilibrium is normally not achieved in each single-stage in industrial counter-current cascades (stage inefficiency).

Continuous counter-current experiments were carried out in Mixer-settler units (MEAB Metalextraktion AB, Sweden). The active volumes of the mixer and the settler were estimated to be 40 and 80 mL respectively. The aqueous feed and the organic phase were fed using electromagnetic pumps (EW-B08TC-20EPF2, EWN-B11TCER, IWAKI, Japan). The pH was controlled by feeding 10 M NaOH in the mixing chamber of each stage using peristaltic pumps (BT103S, Lead Fluid, China). The pH in each stage was measured after sampling a suitable volume of aqueous phase after settling. Details about the pH measurement are given in Section 4.4.
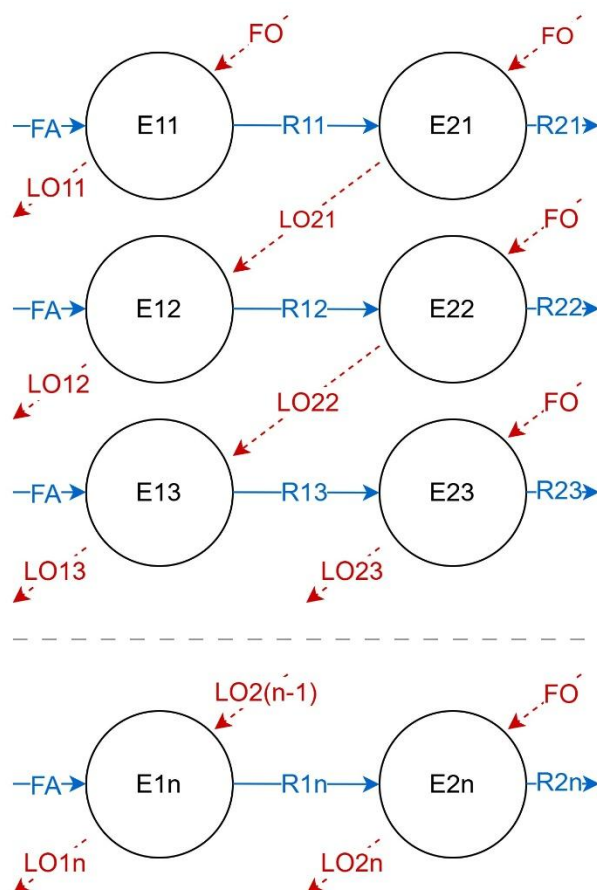

Figure 7. Pseudo counter-current simulation scheme for two stage extraction. Each circle represents one equilibration. FO = Fresh Organic (Solvent), FA = Fresh Aqueous (Feed), R = Raffinate, LO = Loaded Organic. In the nomenclature E11, the stage number is indicated by the first digit, while the second digit and n indicate the number of iterations.

4.3.2 Evaporative Crystallization

Crystallization of metal sulfate salts was performed in a rotary evaporator (RE150-220, Labfirst Scientific, China), at 50 mbar. To remove traces of eventual liquid residues crystals were washed with ethanol (95%) and dried before analysis (T = 60°C, t > 24 h).

4.3.3 Pseudo-ternary Phase Diagrams

Pseudo-ternary phase diagrams for NaOH – extractant – diluent systems were experimentally determined by progressive NaOH titration (<3 wt%) of mixtures with different ratios of extractant and diluent. The samples were prepared in closed glass vials, the mass was recorded after every NaOH addition and mixing was performed using a vortex mixer (VWR international). Monophasic regions have been evaluated adding NaOH until a phase separation was observed by the naked eye (cloud-point method). The phase diagrams obtained in this work are system specific and some variations in the phase behaviours might however occur if the system is modified (e.g., phase modifiers, antioxidants, diluent, base, extractant purity etc.) [94,97–100].

4.4 Characterization Methods

The metals concentration in liquid samples or in solids after dissolution was analysed with Inductively Coupled Plasma-Optical Emission Spectroscopy (ICP-OES, Thermo Fisher Scientific, iCAP™ 6000 Series, USA) and, if required, Inductively Coupled Plasma-Mass Spectroscopy (ICP-MS, Thermo Fisher Scientific, iCAP Q, USA). Y was used as internal standard for ICP-OES measurements, while Sc-45 and In-115 were used for ICP-MS measurements. All the samples were diluted in 0.5 M HNO_3 for the analysis and in the case of ICP-MS filtration was also performed (Syringe filter PTFE – Restek-particle size retention of 0.45 μm).

The pH of the aqueous solutions was measured using a pH electrode (Metrohm 827 pH lab, Metrohm 6.0234.100, Switzerland) calibrated with pH buffers 2, 4 and 7 (Merck, Germany). The redox potential was measured with an ORP electrode (Metrohm 6.0451.100) connected to a 905 Titrando unit (Metrohm). Before use the electrode was tested with a reference solution of 250 mV ($HgCl_2$, Merck, Germany) or of 228 mV at 20°C (Mettler Toledo, USA).

Infrared spectra of organic solvents were recorded using an ATR FT-IR spectrometer Vertex 70V (Bruker). The measurements were performed in the range 4000-450 cm^{-1} with an interval of 4 cm^{-1} and a total of 16 scans.

Viscosity measurements were conducted using an Anton Paar MCR702e Space rheometer (Graz, Austria) equipped with a bob-and-cup measuring geometry (DG27/T200/SS). The measurements were performed in a single motor-transducer configuration. A C-PTD 200 temperature control accessory was used to maintain a constant measurement temperature.

Scanning Electron Microscopy coupled with Energy Dispersive X-ray Spectroscopy (SEM-EDS, FEI Quanta 100 FEG SEM with an Oxford Instruments X-Max EDS detector) was used to investigate the morphology of the solid samples and validate the elemental composition of the solids analysed by ICP techniques.

To identify the crystalline phases of solids, X-ray diffraction analysis (XRD, Bruker D8 Discover) were performed using a Cu source with wavelength 1.5406 Å, 2θ between 10-80°, 15 rpm rotation speed and generator settings of 40 mA and 40 kV. EVA software (Bruker AXS - DIFFRAC.EVA.Version6.0) and JCPDS database (International Centre for Diffraction Data, ICDD,PDF-5+) were used for analytical interpretation.

5 Results and discussions

5.1 Production of High Purity MnSO₄·H₂O from NMC111 LIBs PLS

The composition of the NMC111 PLS used in this work is reported in Table 6. The ionic strength of the solution was 6.5 M, the pH was 5.2 ± 0.1 and the redox potential was 235 mV.

Table 6. Composition of the purified NMC111 PLS. Values for which uncertainty is reported are an average of five different ICP-OES measurements. Fe, Cu and Cd were <LOQ (approximately 0.5, 1 and 0.3 mg/L respectively). F^-, Cl^- and NO_3^- were measured by ion-chromatography. NO_3^- was <LOD (5 mg/L).

	Li	Ni	Co	Mn	Na	SO_4^{2-}	F^-
c (g/L)	4.16 ± 0.09	6.7 ± 0.2	11.2 ± 0.3	10.1 ± 0.2	57.5 ± 1.4	60.3 ± 1.5	0.1
c (mM)	600 ± 10	115 ± 3	190 ± 4	185 ± 4	2480 ± 60	1879 ± 48	5.6
	Al	**Zn**	**Si**	**Mg**	**Ca**	**P**	**Cl^-**
c (mg/L)	34 ± 4	2 ± 1	8 ± 1	11 ± 1	15 ± 5	43 ± 4	25

5.1.1 Extraction of Mn by D2EHPA

The extraction of Mn, Co, Ni and Li by 24% v/v (0.7 M) and 35% v/v (1.05 M) D2EHPA in Isopar L as a function of pH is shown in Figure 8. The batch experiments were performed at $25 \pm 1°C$ and $\theta = 1$ as similar condition were expected to be used in counter-current tests. The contact time was set to 15 minutes based on the available literature [64]. As expected, the extraction of all the metals increased with increasing pH, within the range of pH investigated [84]. When the lowest concentration of D2EHPA was used, Mn extraction above 60% was achieved at pH about 3. The co-extraction of Co, Li, and Ni was, 3, 4, and less than 1% respectively ($SF_{Mn/Co} \approx 25$).
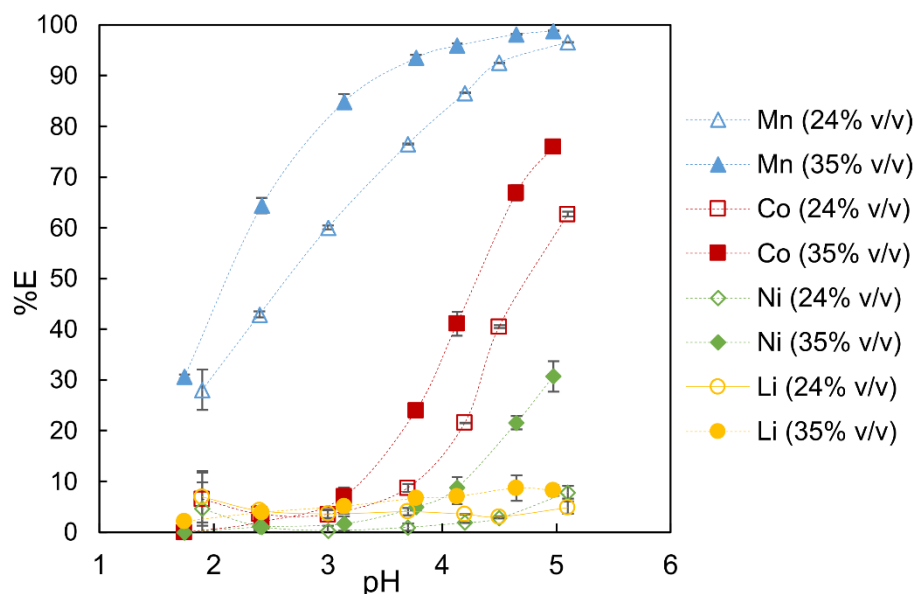

Figure 8. Extraction efficiency as a function of pH for Mn, Co, Ni and Li extracted by D2EHPA in Isopar L (concentration is reported in parenthesis). $\theta = 1$, $t_{eq} = 15$ min, $T = 25 \pm 1°C$, 1000 rpm. Uncertainties of triplicates are shown. The lines do not represent a fit of the points.

Increasing the concentration of D2EHPA enhanced the extraction of Mn, as testified by a shift of the pH_{50} to a lower pH, but favoured the coextraction of the other metals. Accordingly, the slope of the line describing $log(D_{Mn})$ as a function of pH decreases from 0.7 to 0.6 when the concentration of D2EHPA is decreased showing that less molecules of D2EHPA are involved in the extraction of Mn when the lower concentration of extractant is used (Figure 9). A slope of 2, indicating that 2 H^+ are released for each Mn^{2+} extracted would however be expected.
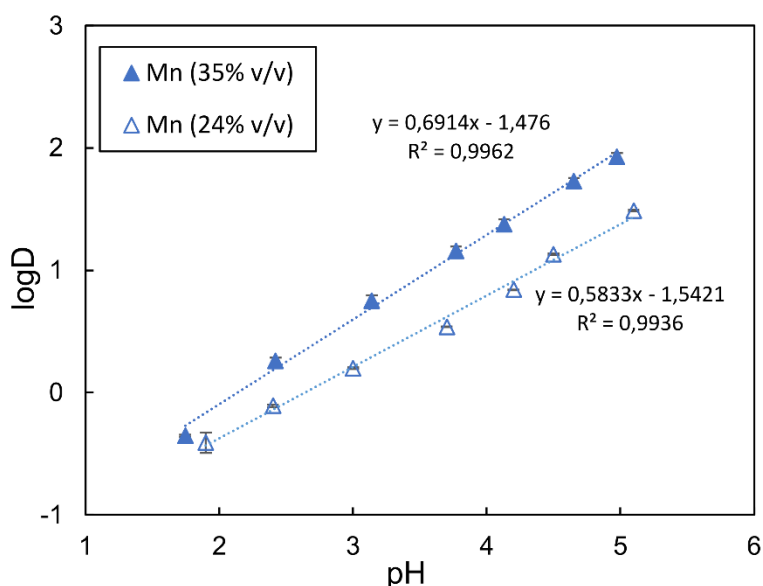

Figure 9. log(D) as function of pH for Mn extracted by D2EHPA 24 and 35% v/v in Isopar L (concentration is reported in parenthesis). θ = 1, t_{eq} =15 min, T = 25 ± 1°C, 1000 rpm. Uncertainties of triplicates are shown.

Satisfactory selectivity could be achieved at pH around 3.1 where almost 85% of Mn was recovered with coextraction of Co, Li and Ni equal to 7, 5 and 2% respectively ($SF_{Mn/Co} \approx 50$). The McCabe-Thiele diagram for extraction of Mn at pH = 3.2 ± 0.1 is shown in Figure 10. Three extraction stages were predicted for extracting 99.9% of the Mn present in the feed at θ equal to 1.

Counter-current extraction was initially performed by stabilizing a constant pH = 3.2 ± 0.1 in all the extraction stages. However, despite achieving complete Mn extraction, significant losses of Co (>15%) were recorded. Consequently, the flow rate of NaOH in the system was reduced and steady state[3] was achieved at pH = 2.9 ± 0.1. More than 98% of Mn was recovered in this condition with coextraction of Co, Li and Ni equal to 4, 5 and 3% (Figure 11a). Further optimization of solvent composition, θ and pH is needed to enhance the performance of the system and avoid excessive Mn contamination of the raffinate. Complete extraction of Ca and Zn was observed in agreement with the expected selectivity of D2EHPA in sulfate systems (Figure 11b) [101]. Furthermore, 60% of Al extraction and 10% of Si and Mg extraction were measured. The concentration of P in the raffinate was measured to be about 30 mg/L higher than the feed suggesting losses of the extractant, and/or some of its impurities, in the aqueous phase. Both mutual solubility and entrainment could be the causes of such increase [84,102–104].

---

[3] According to the conventional theory on residence time distribution, steady state was achieved after more than five cascade volumes were processed [119].

After counter-current operations, the extract contained 8.7, 0.43, 0.08, 0.13 and 0.25 g/L (160, 7, 1, 19 and 11 mM) of Mn, Co, Ni, Li and Na respectively. A slight difference compared to the results of Figure 11 was observed, most likely because of fluctuations in the ICP analysis and/or in the flow rates during operation, as it was carried out on multiple days. The relative purity of Mn in the extract was about 90%, nevertheless higher purity (>99%) is needed to re-use the Mn-rich product as CAM precursor [105]. Scrubbing of the extract is therefore needed.
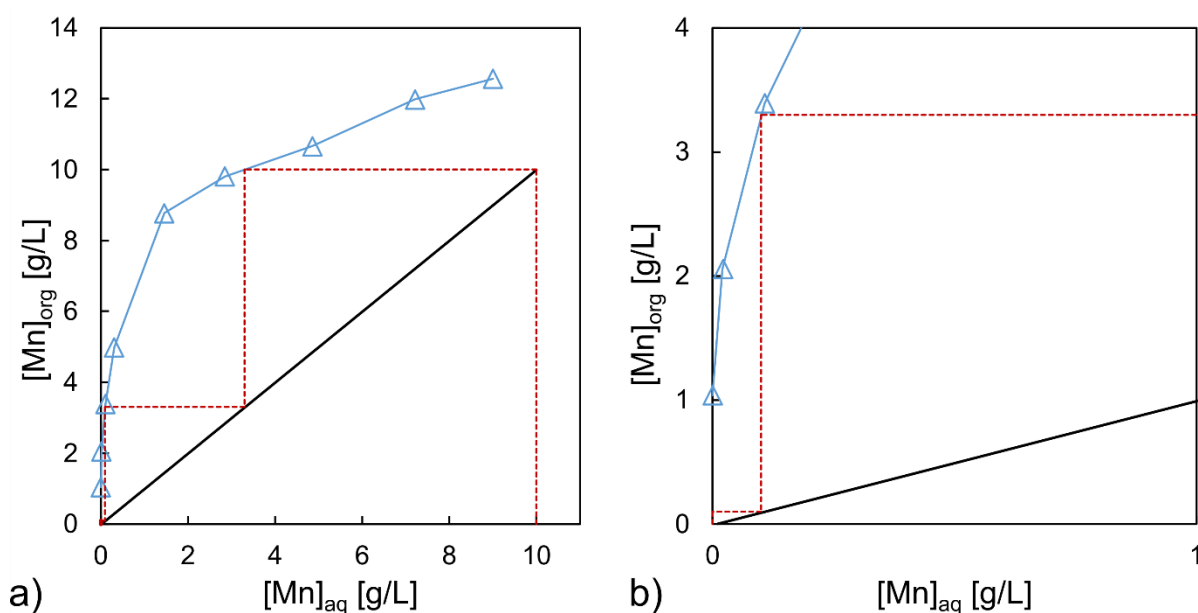

Figure 10. a) McCabe-Thiele analysis applied to equilibrium distribution of Mn between 35% v/v D2EHPA in Isopar L and purified NMC111 feed solution. T = 25 ± 1°C, pH = 3.2 ± 0.1, t_{eq} = 15 min. Initial $[Mn]_{aq}$ = 10.1 g/L. b) Sub-section of the McCabe-Thiele diagram that extends up to $[Mn]_{aq}$ = 1 g/L and $[Mn]_{org}$ = 4 g/L. Operating line calculated for extraction of 99.9% of Mn and θ = 1.
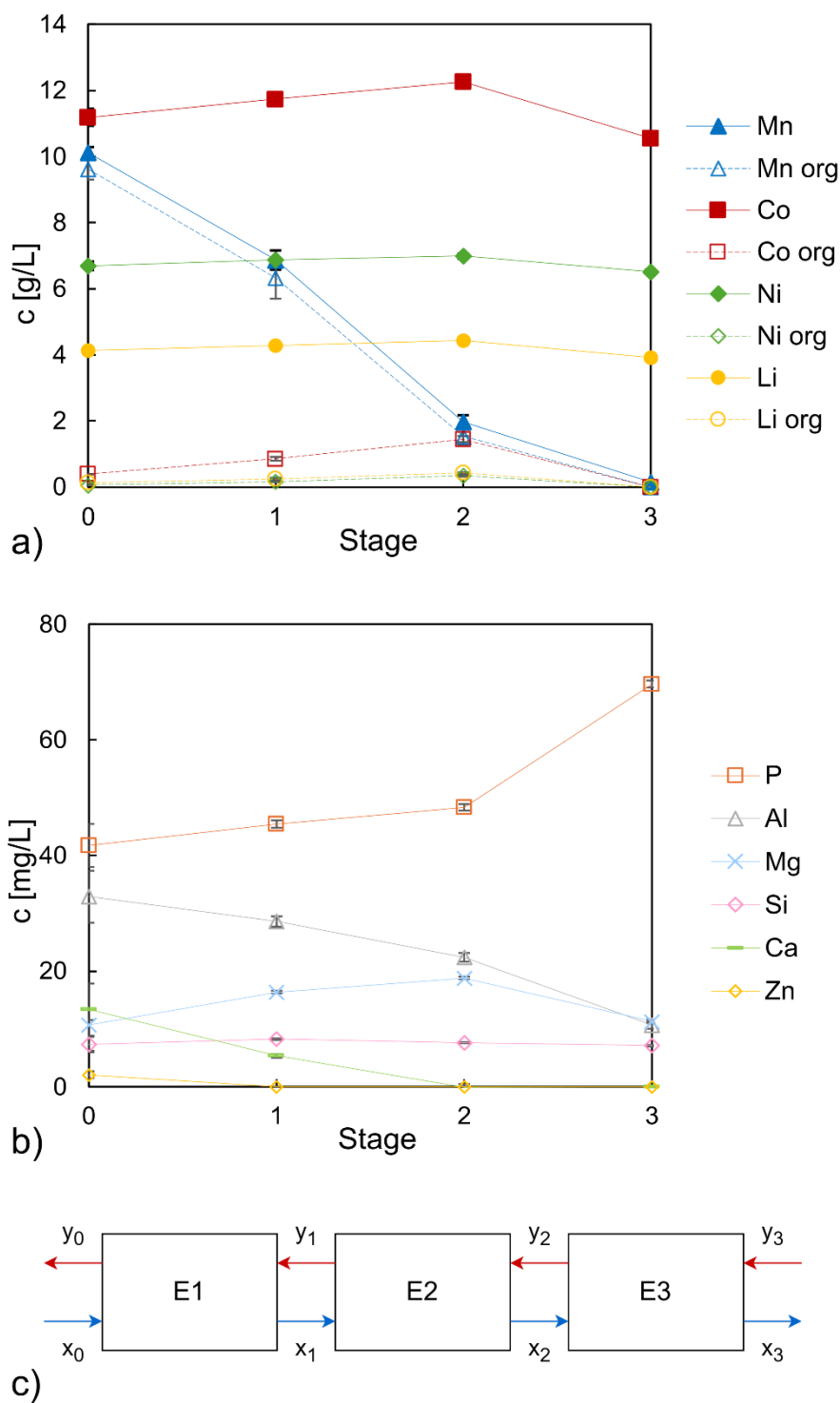
Figure 11. a) Concentrations evolution of Mn, Co, Ni and Li in the aqueous and organic phases and b) concentrations of P, Al, Mg, Si, Ca and Zn in the aqueous phase in a mixer-settler system composed of three stages operated in steady state at pH = 2.9 ± 0.1. 35% v/v D2EHPA in Isopar L, θ = 1, room temperature (23 ± 2 °C). Concentration of the feed solution is reported in Table 1, the concentrations in the aqueous phase are the average of seven samples taken 30 min apart from each other after achieving steady state. Concentrations in the organic phase are an average of three samples taken 1 h apart from each other. Number of stages follows the flow of aqueous phase (left to right). c) Schematic of the counter-current extraction cascade.

5.1.2   Scrubbing and Stripping

In agreement with the available literature [64,106], a Mn-bearing solution was tested to remove the undesired impurities from the extract according to the mechanism shown in Equation (23).

$$M^{\nu+} + \overline{NA_\nu} \rightleftharpoons \overline{MA_\nu} + N^{\nu+} \tag{23}$$
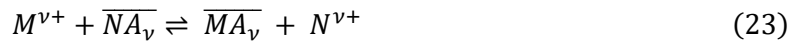
Where *M* is the target metal and *N* represents a generic impurity. The same charge for *M* and *N* was assumed for simplicity. According to Figure 12a, two counter-current stages at θ equal to 1 are needed to remove 99.9% of Co from the extract using a solution containing 4 g/L of Mn (pH = 5.1 ± 0.1). The purified extract produced from counter-current extraction contained 10.4 g/L of Mn and less than 10 mg/L of Co. Li, Ni and Na were all below the respective LOQs. Traces of Mg were found in the aqueous raffinate, whereas no Zn, Al and Ca were detected meaning that these metals were not scrubbed. The concentration of P in the aqueous phase increased also in this case and the pH of the raffinate was 2.8 ± 0.1.
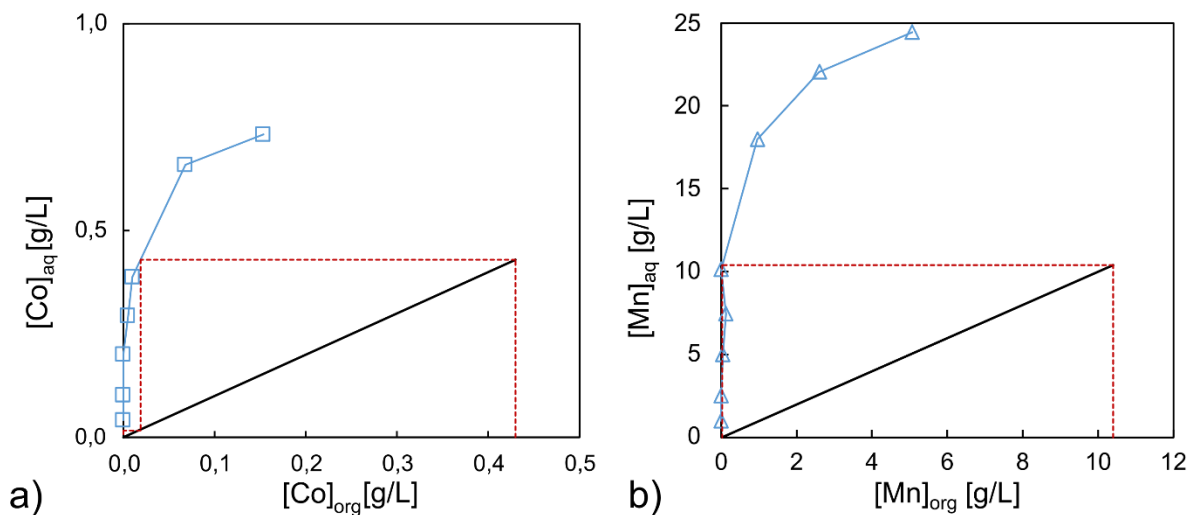

Figure 12. a) McCabe Thiele diagram for scrubbing of the extract using a solution containing [Mn] = 4 g/L. Initial [Co]$_{org}$ = 430 mg/L. Operating line for 99.9% Co scrubbing at θ=1, T = 25 ± 1°C. b) McCabe Thiele diagram for stripping of the purified extract after scrubbing using a solution of 0.5 M H$_2$SO$_4$. Input [Mn]$_{org}$ = 10.4 g/L. Operating line for 99.9% Mn stripping at θ = 1, T = 25 ± 1°C.

An acidic solution was used to strip the purified extract to reverse the equilibrium of the extraction reaction (Equation 11, Page 15). H$_2$SO$_4$ was used since the production of a sulfate salt was targeted. According to the McCabe-Thiele diagram shown in Figure 12b 99.9% of Mn could be stripped in a single stage with θ = 1 using 0.5 M H$_2$SO$_4$. Two counter-current stages were however operated. 99.5% of the Mn was stripped to obtain a product with a relative purity equal to 99.5 ± 0.5% (Table 7). A concentration of Mn lower than the predicted one was measured in the product because the overall θ resulted to be lower than 1 during the operation. The stripped solvent contained 50 mg/L of Mn. Moreover, in contradiction with the expectations, no Al was stripped [107,108]. The impact of the Mn and Al accumulation in the solvent must be evaluated if its recirculation is foreseen. Further optimization is needed, as the recirculation of a fraction of the product as scrubbing agent was not investigated.

Table 7. Composition of the aqueous stripping solution obtained after operation of the mixer settler units. Li, Si and Mg were found in traces (<1 mg/L), while Al, Cd, Ni, Fe and Cu were measured to be below the respective LOQs (0.04, 0.06, 0.1, 0.1 and 0.01 mg/L). Elements concentration is reported as an average of three measurements of the aqueous phase. Cl^- and NO_3^- were measured by ion-chromatography and were both < LOD (1 mg/L). F^- were measured with an ion-selective electrode and were measured to be < LOD (10 mg/L). Uncertainty on purity is computed by propagating the uncertainties on concentration of the single elements. Sulfates are not considered in purity calculations.

	Mn	SO_4^{2-}	Co	Na	Zn	Ca	P	Relative Purity
c (mg/L)	8780 ± 30	15280 ± 340	6 ± 1	1 ± 1	3 ± 1	16 ± 1	14 ± 1	99.5 ± 0.5%
c (mM)	160 ± 4	477 ± 11	/	/	/	/	/	99.4 ± 0.6%

5.1.3 Evaporative Crystallization

To recover Mn as $MnSO_4 \cdot H_2O$, EC was carried out (T = 50°C, P = 50 mbar). Before analysis, filtration and subsequent washing of the crystals with ethanol was necessary as a liquid residue was present together with the solid product after the operation (~80 mL from 3.7 L of initial solution). Such residue contained more than 7 M of S, 3 g/L (55mM) of Mn and 100 mg/L (3mM) of P. Since the molar ratio of Mn^{2+} and SO_4^{2-} in the expected $MnSO_4 \cdot H_2O$ crystals is equal to 1, an excess of 0.32 M of sulfates compared to the total quantity of Mn in the stripping product can be computed (Table 7). The high S content in the residue suggests that the excess sulfuric acid contained in the stripping product was concentrated in the liquid residue during crystallization. The presence of P suggests that the same happened to the D2EHPA and, eventually, its main impurities (M2EHPA, T2EHP, and 2-ethylhexanol) which were present in the product. Their boiling point is indeed higher than the one of water [109–112]. Removal of the organic residues from the product, alternative crystallization techniques might be considered, and the minimization of excess acid used for stripping might help in minimizing the quantity of liquid residue [55,86]. Losses of Mn in the residue below 1% were estimated.

The XRD pattern confirmed that monohydrated $MnSO_4$ was produced (Figure 13). The relative purity of the product was 99.6 ± 0.1% according to ICP analysis (Table 8). However, no P was detected and quantification of Fe, Al and Si with such technique was not possible due to matrix interferences. Weak signals indicating the presence of traces of Si and P (<0.1 wt%) were however obtained from SEM-EDS measurement (Publication 1, Figure 8). A comparison between the elemental composition of the obtained product and the purity requirements reported by [105] is shown in Table 8. According to such values, the requirements for Mn, Cu, Cd and Mg content were fulfilled. The content of Na, Ca and Zn in the produced salt exceeded the target values instead. However, as NaOH is normally used to precipitate the pCAM from the solution containing the dissolved transition metals salts, its presence in the product is not expected to have a significant impact on the process [19,113]. Despite the indications provided by [105], in some cases the presence of impurities has even been reported to not impact or to be even beneficial for the newly synthesised CAM [105,114–116]. This reflects the lack of clarity that characterizes the literature available on the topic. Figure 14 shows the flowsheet of the proposed combined SX and EC process.

Table 8. Comparison between composition (wt%) and purity of the produced MnSO₄·H₂O and requirements (wt%) for battery grade MnSO₄·H₂O according to [105]. Uncertainty of the metals wt% is computed from triplicates. Uncertainty of the purity is obtained by uncertainties propagation.

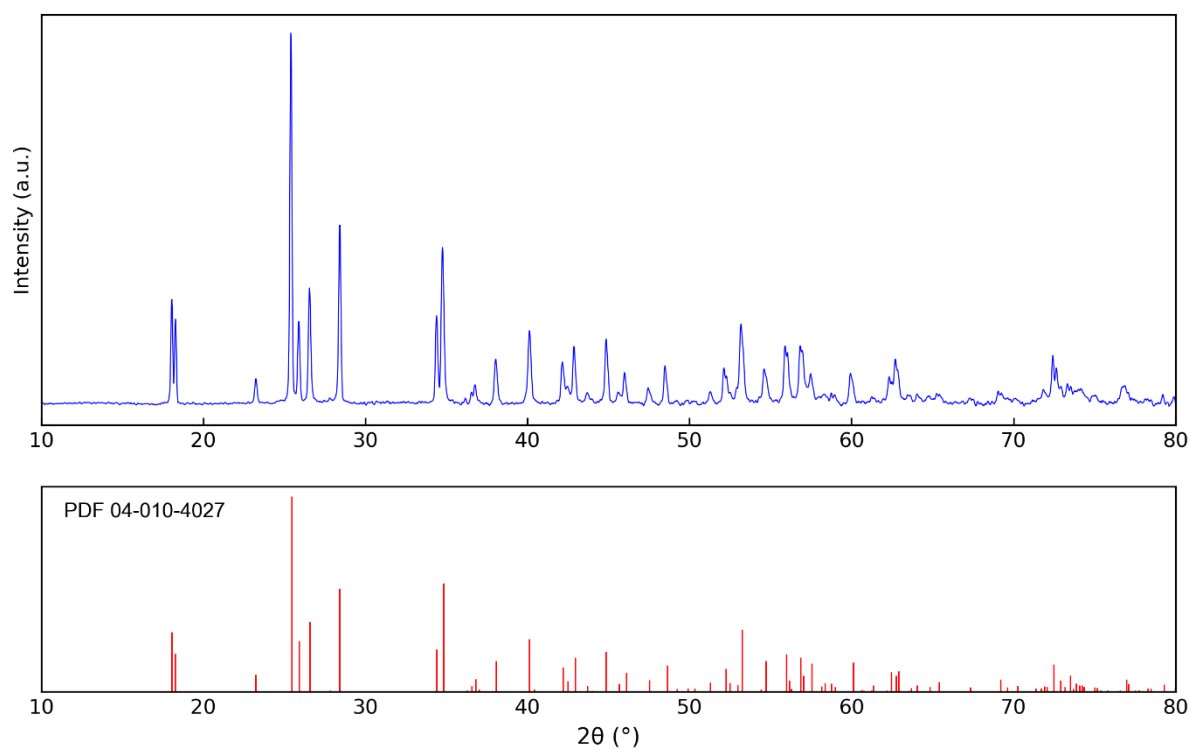|	**MnSO₄.H₂O Product (wt%)**	**Requirements**
Mn	32.39 ± 0.03	≥ 32
Co	0.025 ± 0.001	/
Ni	0.003 ± 0.0001	/
Li	0.001 ± 0.00001	/
Na	0.016 ± 0.006	0.005
Zn	0.010 ± 0.00004	0.001
Mg	0.0021 ± 0.00003	0.005
Ca	0.063 ± 0.002	0.005
Cu	0.0004 ± 0.00002	0.001
Relative Purity	99.6 ± 0.1 %	/

Figure 13. X-ray diffraction pattern of MnSO₄·H₂O product. Comparison is made with PDF 040-010-4027 for the same compound. Crystalline structure: monoclinic. Plot re-drawn from Paper 1 Figure 7 [117].
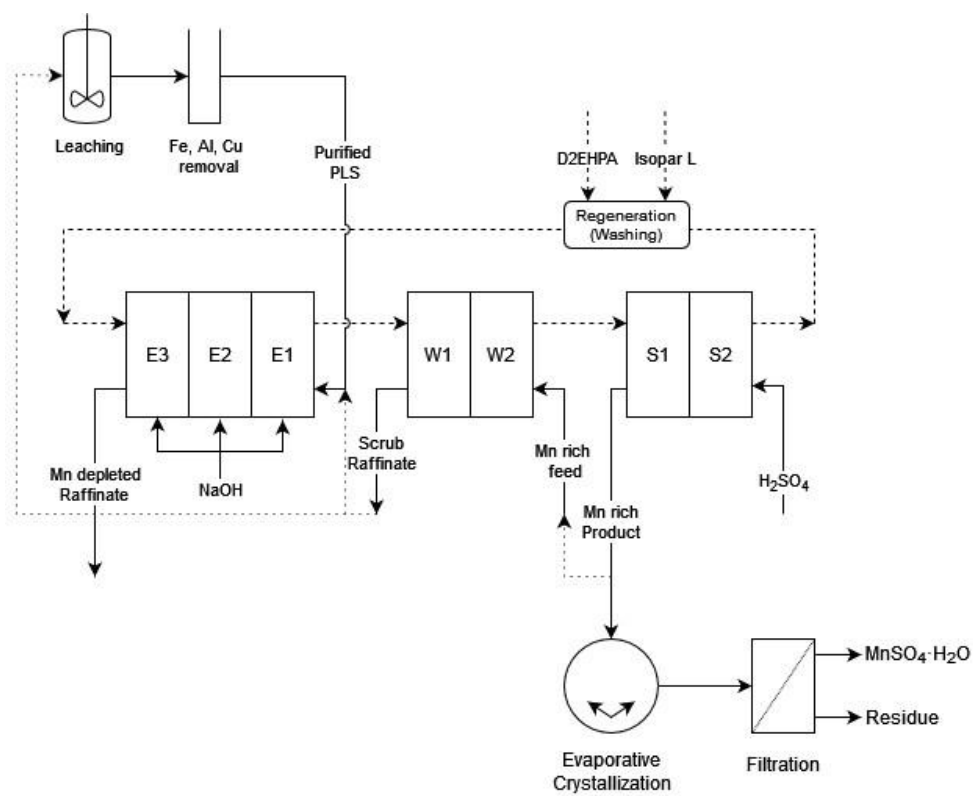
Figure 14. Mn solvent extraction and crystallization flowsheet. Dashed lines represent the flow of organic streams. Dotted lines represent options for streams recirculation.

5.1.4 Summary

The main results obtained in this work (Paper I) can be summarized as follows:

- 98% of Mn was recovered from a NMC111 PLS using 35% v/v D2EHPA in Isopar L in three counter-current stages at pH = 2.9 ± 0.1 and θ = 1. The co-extraction of Co, Ni and Li was respectively 5, 3 and 4%.
- Almost complete Co removal (97%) was achieved by counter-current contact of the extract with a 4 g/L solution of Mn in two stages at θ = 1. Ni and Li content in the extract was measured to be below their LOQs.
- 99.5% of the Mn contained in the extract was stripped using 0.5 M H_2SO_4 in two stages at θ = 1 to obtain a product of relative purity equal to 99.5 ± 0.5%.
- $MnSO_4 \cdot H_2O$ with a relative purity of 99.6 ± 0.1% (Mn > 32 wt%) was crystallized.
- A liquid residue containing H_2SO_4, traces of the dissolved solvent and a small fraction of Mn was concentrated during evaporative crystallization.

Concerning the distribution of metallic impurities in the system (Ca, Zn, Mg, Na, Si, and Al), the following was observed:

- Ca and Zn were completely extracted from the feed, could not be scrubbed and ended up in the final product in a quantity that exceeds the limits for battery grade $MnSO_4 \cdot H_2O$ reported by [105].
- Mg was partially extracted (10%) but could be scrubbed from the extract and its final content in the product met the requirements reported by [105].
- The extraction of Na could not be quantified as NaOH was added to the system for pH adjustment. However, despite being quantitatively scrubbed, traces of Na remained in the produced salt but are not expected to affect the quality of the pCAM if its co-precipitation is performed by addition of NaOH.
- Al was partially extracted (60%) and could not be scrubbed or stripped. Its concentration in the final product was below LOQ based on ICP-OES measurement and could not be quantified using ICP-MS because of matrix interferences.
- Partial extraction of Si was observed (10%) but no further information could be obtained on its behaviour due to its low concentration and the impossibility to measure such element with ICP-MS due to the interference of the Si coming from glass containers.

5.2 Phase behaviour of saponified Cyanex 272 and counter-current extraction of Co(II) from Ni-rich spent LIBs leachate

As all the extractants used in this work are acidic, pH control is fundamental to achieve the desired selectivity. In Paper I, direct addition of NaOH to the extraction stages was performed and confirmed to be a challenging operation. In alternative to the direct addition of NaOH, saponification of the solvent (Equation 19, Page 16) can be performed and is generally considered the simplest solution to the pH control problem [73]. This operation reduces the risk of local supersaturation linked to the addition of concentrated NaOH in the system and facilitates counter-current operation. Particular attention in understanding how to use a saponified solvent in counter-current SX and how to choose suitable saponification conditions was paid in Manuscript II since such kind of information is not easily available in the literature. Extraction of Co from the raffinate obtained in Paper I was tested. However, Na_2SO_4 precipitation was observed when the pH was raised (Appendix A). The extraction of Co with saponified Cyanex 272 was therefore investigated using another available feed produced from NMC9.5.5 LIBs (Table 9). The ionic strength of the solution was 5.6 M, the pH was 3.4 ± 0.1 and the redox potential was 355 mV.

Table 9. Concentration of the main elements contained in the NMC9.5.5 PLS after Mn removal. Values for which uncertainty are reported are averages on 15 samples. The concentrations before Mn removal can be found in (Appendix B).

	Co	Ni	Li	Mn	Na	SO_4^{2-}	P
C (g/L)	3.12 ± 0.05	41.1 ± 0.6	5.74 ± 0.07	0.01 ± 0.00	22.2 ± 0.26	52.0 ± 0.8	0.08 ± 0.00
C (mM)	53 ± 1	700 ± 10	827 ± 10	<1	964 ± 11	1622 ± 25	2.5 ± 0.1

5.2.1 Selection of saponification conditions

Before proceeding with testing Co extraction, the effect of the concentration of NaOH and temperature on the solvent phase behaviour and viscosity were investigated to select appropriate saponification conditions for the Cyanex 272 – Isopar L mixture that will be used for Co SX.

Figure 15 shows the pseudo-ternary diagrams for the system NaOH - Cyanex 272 - Isopar L for 2, 5 and 10 M NaOH at $T = 21 \pm 2°C$ and 10 M NaOH at $40 \pm 1°C$. The dashed lines delimit the area of the diagram experimentally determined, which correspond to the area of interest for the phase behaviour of the pre-neutralized solvent. Three domains were identified in such area of the diagrams:

- 1φ: monophasic region
- 2φ: biphasic liquid-liquid region with a hydrophilic and a hydrophobic phase.
- 2φ*: biphasic liquid-liquid region with diluent rich (light) and diluent depleted (heavy and viscous) phases.

Starting from the Cyanex 272 - Isopar L axis and moving towards the NaOH vertex, the initially monophasic solvent becomes biphasic (2φ) when NaOH is added. The quantity of NaA present in the system at low *N* is indeed not sufficient to solubilize all the added water [118]. After further addition of NaOH, the system returns monophasic (1φ) and eventually separates in a diluent-rich and diluent-poor phase (2φ*) (Appendix B). Negligible variations in the phase behavior were observed when the temperature increased from 21 to 40°C in the case of 10 M NaOH (Figure 15c-d). Increasing the temperature during saponification might however be considered if a reduction in the viscosity of the solvent is foreseen (Appendix B).

As expected, a shift of the region of interest of the diagram towards the Cyanex 272 – Isopar L axis was

observed when the NaOH concentration was increased since a lower quantity of NaOH needs to be added to the solvent to achieve the same degree of saponification [98,99]. The obtained diagrams are coherent with the available literature, except for the absence of the isothermal invariant point [99,118].
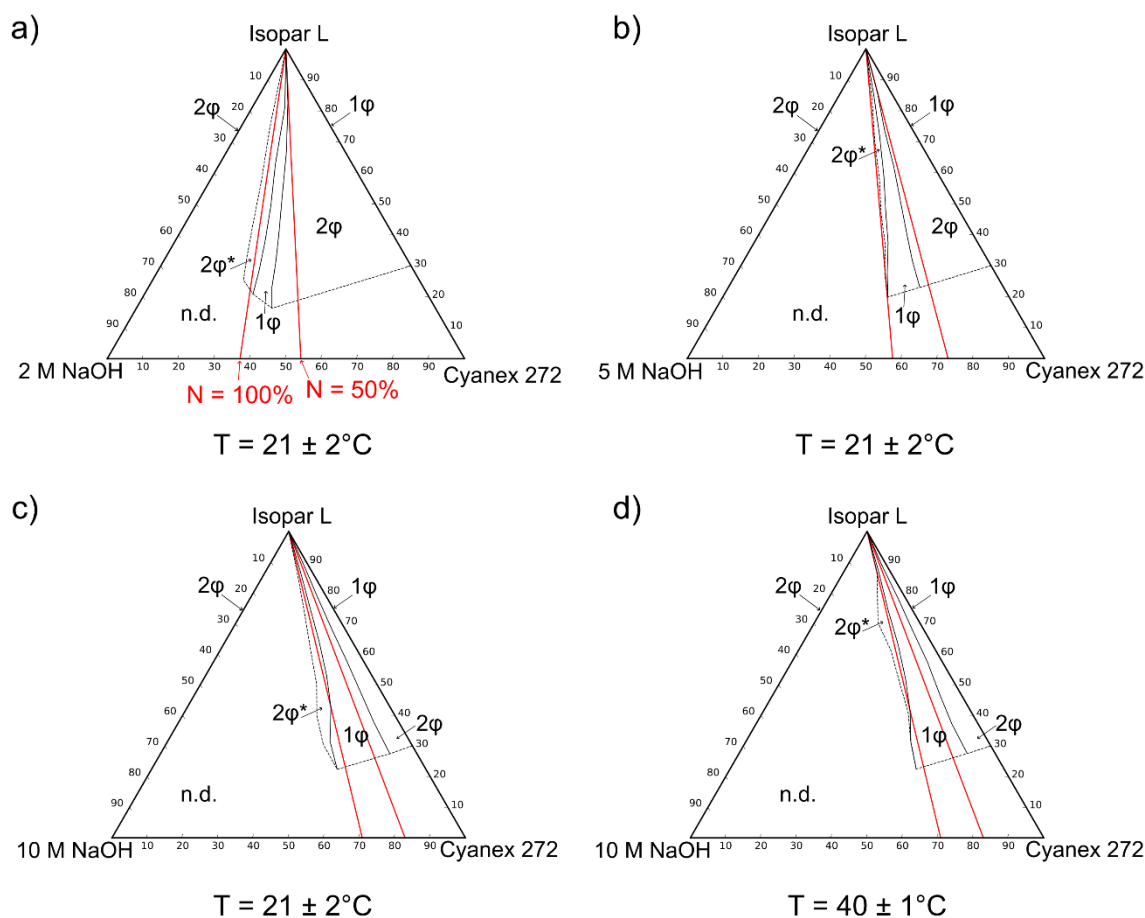

Figure 15 Pseudo-ternary phase diagrams for the system NaOH - Cyanex 272 - Isopar L at different NaOH concentrations and temperatures. a) 2 M NaOH T = 21 ± 2°C; b) 5 M NaOH T = 21 ± 2°C; c) 10 M NaOH T = 21 ± 2°C; d) 10 M NaOH T = 40 ± 1°C. Concentrations are given in wt%. The black dashed lines delimit the region of the diagram that was determined experimentally. The red lines represent a theoretical pre-neutralization degree (N) of 50% and 100%. n.d. stands for not determined.

A zoomed-in fraction of the phase diagrams shown in Figure 15a-c is shown in Figure 16. Improved stabilization of the microemulsion region can be observed when the concentration of NaOH is increased because of the higher NaA/H$_2$O ratio (Equation 19, Page 16) [118]. For instance, when $N = 40\%$, the solvent is monophasic when 10 M NaOH is used but it is biphasic when the concentration of NaOH is 2 or 5 M.

The effect of the relative extractant/diluent content on the phase behaviour of the system can be observed by looking at the phase transition lines. For 2 M NaOH, the line describing the transition from 2φ to 1φ shifts towards higher N when the content of extractant in the system is increased. Such shift becomes less relevant as the concentration of NaOH is increased, and the total volume of water in the system is reduced. A similar effect can be observed for the transition from 1φ to 2φ*, which indicates the limit condition for which the solvent can be used for SX. Such transition takes place at $60 \leq N < 100\%$ in the case of 2 M NaOH, $70 \leq N < 100\%$ in the case of 5 M NaOH and finally for $N \geq 80\%$ or even $N > 100\%$ if 10 M NaOH is used suggesting that a higher concentration of NaOH allows to achieve a higher saponification degree before the solvent becomes unsuitable for SX purposes.
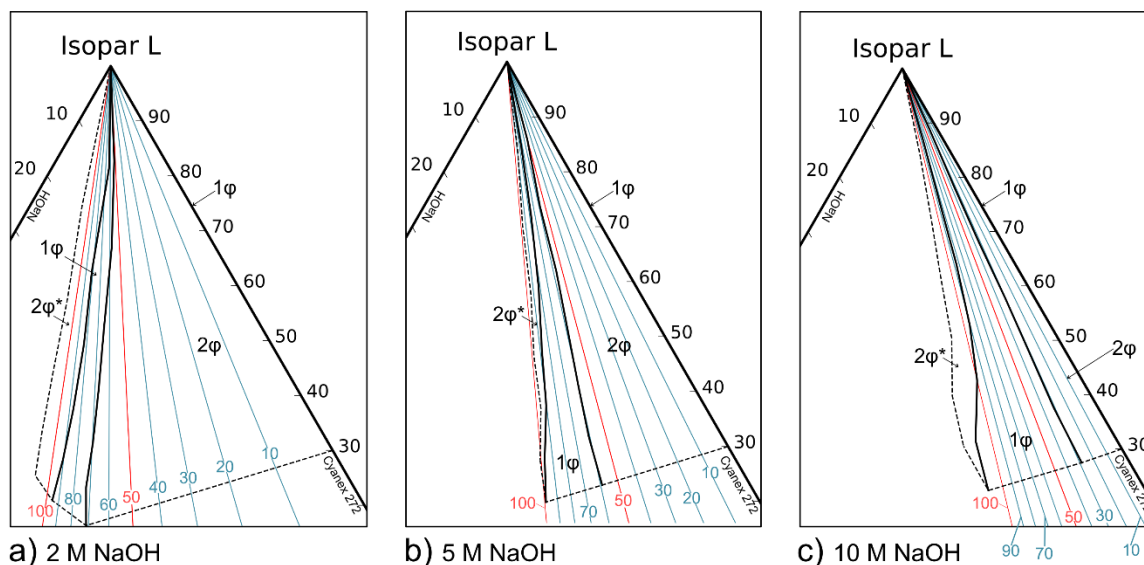
Figure 16. Section of the pseudo-ternary phase diagrams for the system NaOH - Cyanex 272 - Isopar L at different NaOH concentrations and T = 21 ± 2°C. a) 2 M NaOH; b) 5 M NaOH; c) 10 M NaOH. Concentrations are given in wt%. The black dashed lines delimitate the region of the diagram that was determined experimentally. The blue and red lines represent the theoretical pre-neutralization degree (N) as indicated by the numbers.

As discussed above, the solvent can be used for SX when, after saponification, it exhibits biphasic (2φ) or monophasic (1φ) behaviour. The amount of aqueous phase introduced in the solvent by addition of NaOH and its eventual impact on the phase ratio of the final SX system might drive the selection of a suitable concentration of base. If the content of aqueous phase is high enough to significantly impact the phase ratio of the SX system, separation of the two phases must be carried out in the case in which the solvent is biphasic. However, variations of the phase ratio cannot be avoided if microemulsions are formed and the solvent is monophasic. During the extraction of multivalent ions, reverse micellar aggregates are indeed expected to break and release their aqueous core in the aqueous layer [93]. If the content of aqueous phase in the solvent is low enough to have a negligible impact on the phase ratio of the SX system, no issues relative to the use of a solvent containing microemulsions should be encountered and, in principle, separation of the hydrophilic and hydrophobic phase could be avoided if the saponified solvent is biphasic. However, as done by *Jantunen et al.* [119], stirring of the biphasic solvent might be performed to form a homogeneous kinetically stable emulsion before SX.

An idea of the amount of water added to the solvent for different saponification conditions can be derived from the phase diagrams. For a fixed *N*, the amount of water added increases with increasing content of Cyanex 272 and decreasing NaOH concentration. The use of high concentrations of NaOH seems to be advantageous to minimize the water content in the system and achieve high N. On the other hand, the tendency to stabilize microemulsions is a disadvantage if the amount of water contained in the solvent impacts the phase ratio of the system. In such case, lowering the concentration of NaOH might favour the formation of a biphasic saponified solvent and allow separation of the hydrophobic and hydrophilic layers. This would be however advantageous only in the case in which the water content of the hydrophobic phase is lower than the one of the microemulsion which would form by saponifying with more concentrated NaOH. Moreover, this issue might be faced only when high *N* and high concentration of Cyanex 272 are used. Other challenges, such as an increased viscosity of the solvent might also arise in such conditions.

In this work, extraction of Co was initially carried out using 12 wt% Cyanex 272 (0.3 M BTMPPA) in Isopar L at θ equal to 1 ([HA]/[Co] ≃ 6, L ~ 40%). The content of water in the solvent at $N = 80\%$ was estimated to be below 3% if 10 M NaOH is used for saponification, therefore such concentration of base was initially selected to saponify the solvent. Saponification was performed at $21 \pm 2°C$ as no need for a temperature increase during saponification was observed and all the SX experiments were performed at such temperature.

5.2.2   Extraction of Co, Ni and Li by saponified Cyanex 272

Before proceeding with testing the extraction of Co as a function of N and pH, the kinetics of the system was studied. The viscosity of the solvent increased from 1.8 mPa·s for the fresh solvent to 2.6 and 5.2 mPa·s when N equals 70 and 80% (Table 10). Such variation in the rheological properties of the fluid were considered to have a negligible impact on the mass transfer, in agreement with the results obtained by *Vieceli et al.* for 0.4 M Cyanex 272 in Isopar L (N = 10 - 60%) [70]. Therefore, the kinetics for Co, Ni and Li extraction was tested only for $N = 40\%$ (Figure 17a). Co extraction reached equilibrium after 5 min. The low distribution ratio of Li and Ni did not allow to gather any relevant information. The presence of Mn in the raffinate could not be quantified using ICP-OES ([Mn] < LOQ = 0.04 mg/L), therefore no extraction data is reported.

Table 10. Viscosity of 12 wt% Cyanex 272 (0.3 M BTMPPA) in Isopar L as a function of the degree of pre-neutralization (N) at T = 21 ± 1°C, [NaOH] = 10 M. The values reported for viscosity are an average over more than 10 shear rates in the range 0.63-100 s⁻¹ and the uncertainty is <0.05 mPa·s in all cases. When the system was biphasic (N = 10, 20%), the viscosity of the upper (hydrophobic) layer was measured.

N (%)	0	10	20	30	40	50	60	70	80
η [mPa·s]	1.8	1.8	1.8	1.9	1.9	2.1	2.2	2.6	5.2

Figure 17b shows the extraction of Co, Ni and Li by saponified Cyanex 272. Smooth phase disengagement was achieved in all cases and negligible changes in the phase ratio were observed (deviation from mass balance < 5%). Increasing N resulted in an increased pH favouring the extraction of the metals. For all the N tested, the equilibrium pH of the system was higher than the initial pH of the feed solution.

Keller et al. [66] suggest that at pH lower than the extractant's pKa, the dissociation of the extractant sodium salt (NaA) might favour the recombination of the free A⁻ with a proton and therefore increase the pH of the aqueous layer. However, due to the dependency of the extractant pKa on the system, the lack of information about the equilibria of BTMPPA with its sodium salt and the simultaneous extraction of other metals (Mn, Co, Ni, Li) it is complex to define if the recombination of HA is the main responsible for the pH increase [63,91,120–122].
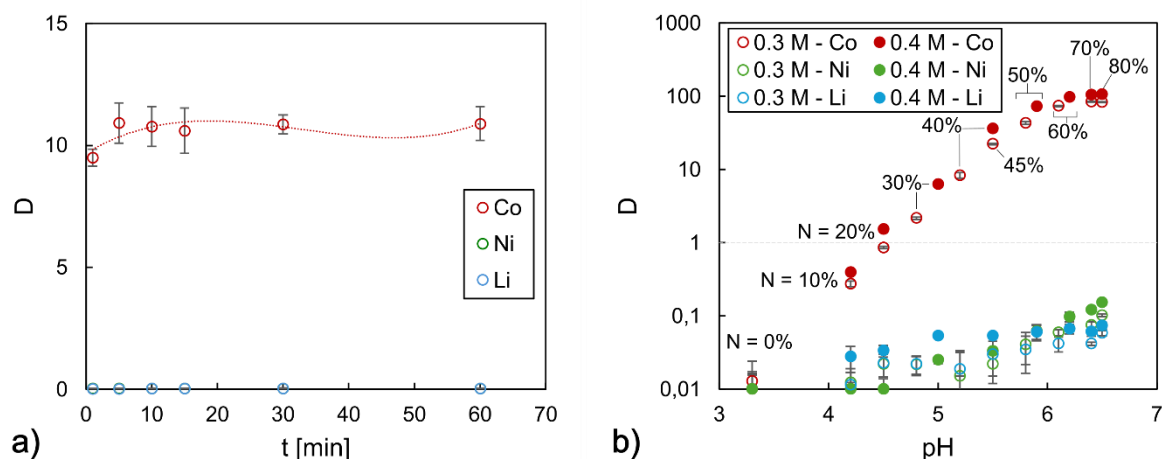
Figure 17. Distribution ratio of Co, Ni and Li. (a) as a function of time for 0.3 M Cyanex 272 in Isopar L (N = 40%), pH$_{eq}$ = 5.2 ± 0.1. (b) Distribution ratio of Co, Ni and Li as a function of pH and N for 0.3 and 0.4 M Cyanex 272 in Isopar L. In all the tests, θ = 1, T = 21 ± 2°C, t$_{eq}$=15 min. Uncertainties of triplicates are shown.

The rupture of reverse micellar aggregates during the extraction might also contribute to the pH variation. Reverse micelles or microemulsions are indeed formed when NaOH is added to the solvent during saponification. As Na is released in the aqueous phase during the extraction, such aggregates are broken and their aqueous core, which might also contain unreacted NaOH, is most likely released into the heavier phase. The FTIR spectra of 0.3 M Cyanex 272 before and after saponification and after extraction of Co for N = 80% is shown in Figure 18. The presence of the OH stretching vibration band (3400 cm^{-1}) and the HOH bending vibration peak (1640 cm^{-1}) indicate the presence of water in the microemulsions formed at N = 80% [123,124]. The rupture of the reversed micellar systems is confirmed by the absence of these peaks in the spectra of the Co loaded solvent. A shift in the peaks related to the P=O (1170 cm^{-1}) and P-OH (958 cm^{-1}) bonds are also visible both after saponification and Co extraction due to the formation of Na and Co complexes with BTMPPA [125].

At pH higher than 6, the distribution ratio of Co seems to reach a plateau. Possible explanations might be the reached solubility of the extracted Co complex in the solvent or competition with Ni and Li extraction. The presence of the flocculants and the high concentration of metals in the feed makes it difficult to assess if a change in Co speciation might also be involved. No significant enhancement in Co recovery was observed when the concentration of Cyanex was increased from 0.3 to 0.4 M (Figure 17b). 0.3 M Cyanex 272 and N = 45% were selected for the counter-current tests. In this condition, 95% of Co (D$_{Co}$ = 22.4 ± 0.5) could be extracted in a single stage at pH of 5.5 ± 0.1. All the Mn was co-extracted together with less than 4% of Ni and Li. Considerable Ni contamination of the extract might be expected even if low extraction is measured as the initial concentration of such metal is much higher than Co (Table 9, Page 34).
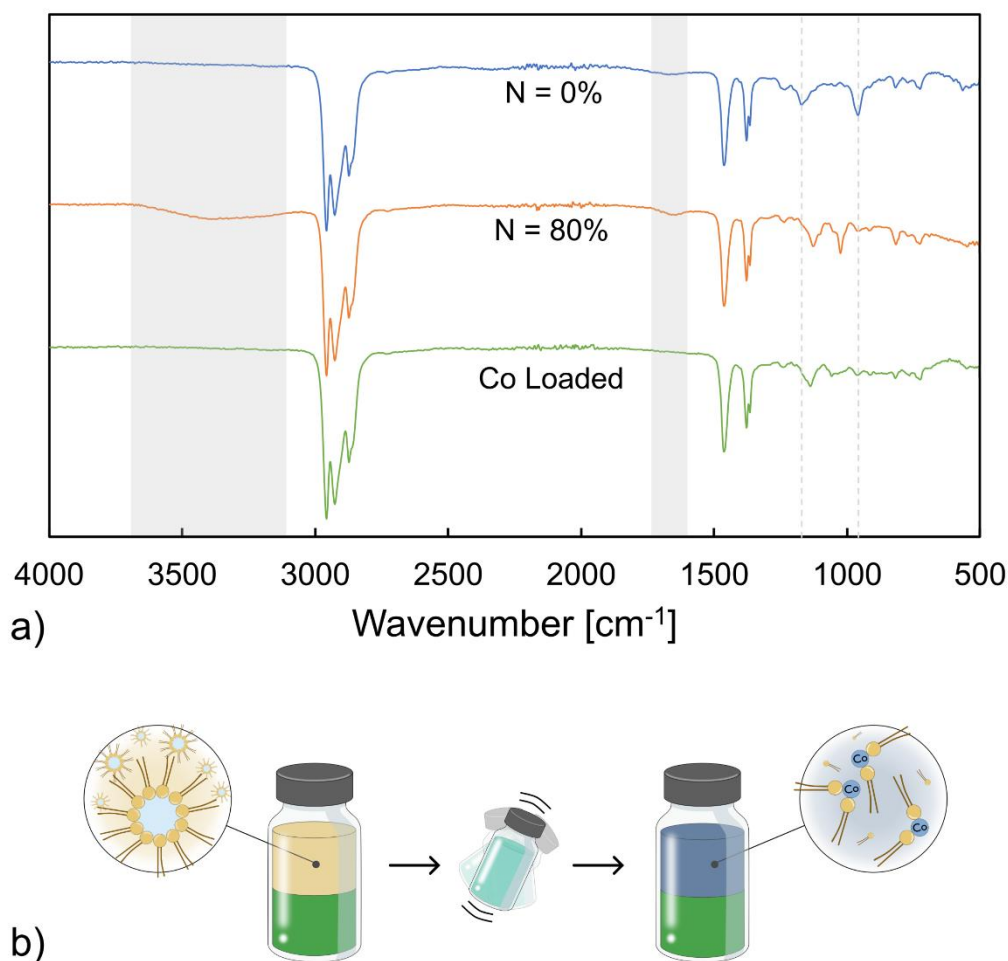
Figure 18. a) FTIR spectra of 0.3 M Cyanex 272 in Isopar L before saponification (Fresh, N = 0%), after saponification (N = 80%), and after Co extraction (Co Loaded). The dotted lines indicate the wavenumber corresponding to P=O and P-O-H stretching vibrations of Cyanex 272 (1170, 958 cm^{-1}). The grey bands indicate the OH stretching vibration band (3400 cm^{-1}) and the H-O-H bending vibration peak (1640 cm^{-1}). b) Graphical representation of the rupture of the reverse micellar systems after the extraction of Co.

5.2.3   Determination of number of extraction stages and pseudo-cc tests

In agreement with the methodology adopted in the available literature, a McCabe-Thiele diagram with a 45% saponified solvent was built to determine the number of counter-current stages needed to extract Co [71,73]. The extraction isotherm obtained by contacting the feed and the saponified solvent at different θ is characterized by a peak at $[Co]_{org}$ = 3.2 g/L (Figure 19a). The presence of a pinch point when an operating line for 99.9% extraction of Co at θ = 1 is drawn suggests that complete extraction of Co is theoretically not possible in such conditions. Since in single-stage extraction the system reaches equilibrium at pH = 5.5 ± 0.1 when 45% saponified Cyanex 272 is used, an extraction curve was obtained contacting the feed and the solvent at different θ with a constant pH of 5.5 ± 0.1 (Figure 19b). Similar trends in the two extraction isotherms can be seen up to a $[Co]_{org}$ = 3.0 g/L. No pinch point is however observed in the second case and two stages seems to be needed to extract 99.9% Co at θ equal to 1 and pH = 5.5 ± 0.1. The variation in equilibrium pH that occurs when the 45% saponified solvent is contacted with the feed at different θ might explain such discrepancy (Figure 19c). As the pH decreases with decreasing θ, the extraction of Co is hindered (Equation 11, Page 14) resulting in a peak shaped extraction isotherm.
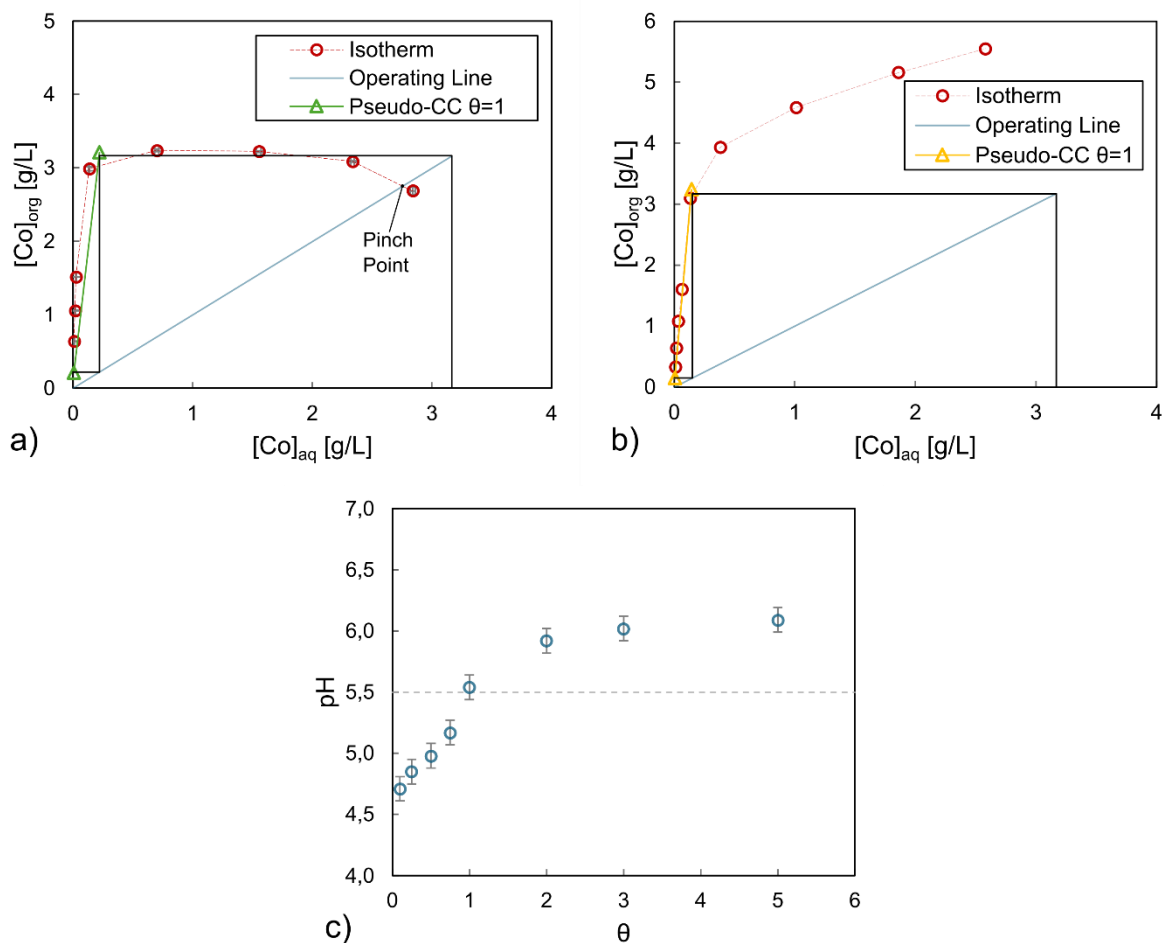
Figure 19. Comparison between Co extraction isotherms obtained with McCabe-Thiele method and pseudo-cc by 0.3 M Cyanex 272 in Isopar L (a) at N = 45% and (b) at pH = 5.5 ± 0.1. (c) Equilibrium pH as a function of θ for Co extraction by 0.3 M Cyanex 272 in Isopar L (N = 45%). T = 21 ± 2°C, t_{eq}=15 min. Feed composition in Table 9. In all cases the operating line is drawn for 99.9% Co extraction and θ = 1. Uncertainties of triplicates are shown.

The comparison between the equilibrium points for the extraction performed using 45% saponified solvent and the extraction isotherm obtained with the McCabe-Thiele methodology in shown Figure 19a. The inaccuracy of the McCabe-Thiele method in describing the cascade equilibria is confirmed. Approximately 99.8% of Co was recovered in two counter-current stages using 45% saponified 0.3 M Cyanex 272 (Table 11). Almost identical extraction of Co, Ni and Li was observed when a two stage pseudo-cc test was performed with non-saponified extractant and by adjusting the pH to 5.5 ± 0.1 in both stages. In the latter case, good agreement between the equilibrium data and the McCabe-Thiele diagram was observed (Figure 19b).

The equilibrium concentrations of Co, Ni and Li show similar trends in both the pseudo-cc tests that were carried out (Figure 20). However, due to the different pH at which the two stages equilibrate, a higher concentration of metals can be observed in the raffinate of stage one (x_1) and in the extract of stage 2 (y_1) when the saponified solvent is used. This is evident in the case of Ni due to its high concentration while it is almost negligible for Co. As expected, a gradual increase in the Na concentration in the aqueous phase is shown when the pH is adjusted to 5.5 in all the stages by NaOH addition, while when the saponified solvent is used almost all the Na is released at the first contact with the aqueous phase (stage 2). In both cases the total amount of NaOH added to the system accounts for less than 0.5% of the total cascade volume.

Table 11. Extraction efficiency of Mn, Ni and Li and concentration of Mn, Ni, Li and Na in the raffinate and extract of the countercurrent pseudo-cc tests performed with saponified solvent (N = 45%) and by adjusting the pH to 5.5 ± 0.1 in both stages (N = 0%). The uncertainty on the relative purity is computed by uncertainty propagation.

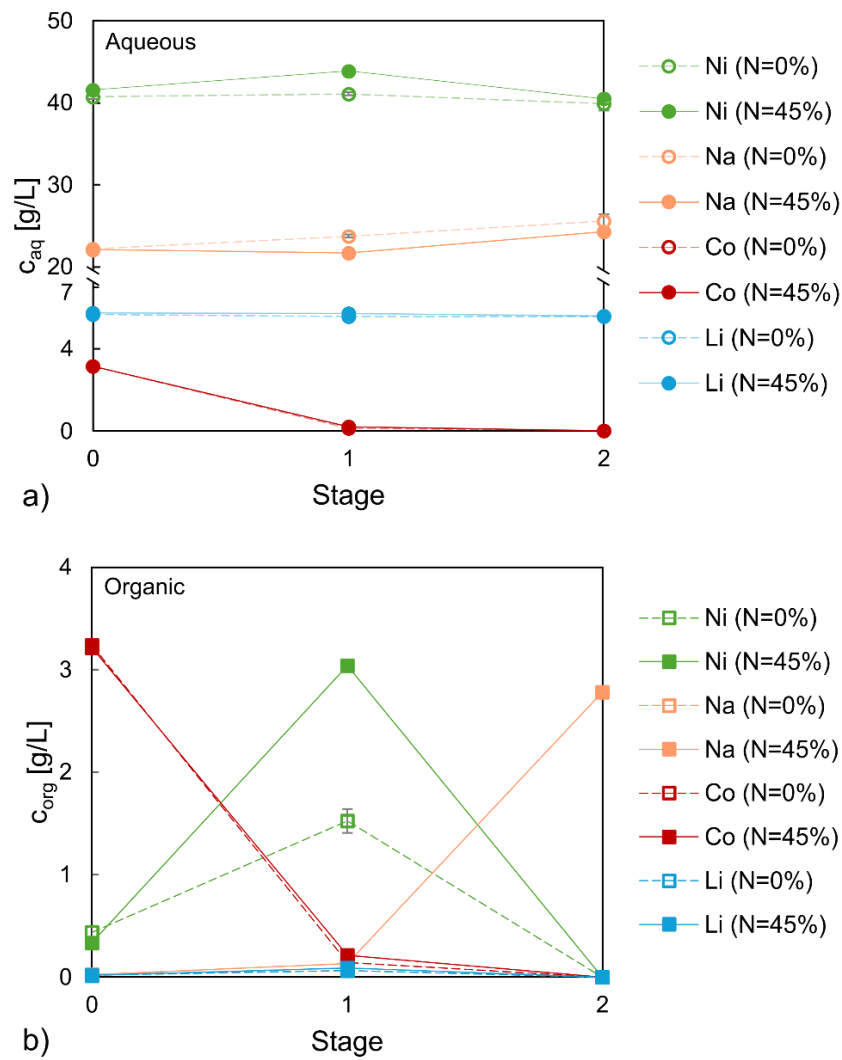| Solvent	pH		Raffinate				Extract					$\%E_{Co}$	$\%E_{Ni}$	$\%E_{Li}$
			[mg/L]	[g/L]			[g/L]	[mg/L]			$P_{R,Co}$			
	E1	E2	Co	Ni	Li	Na	Co	Ni	Li	Na				
N = 45%	5.4	5.9	7	40.5	5.6	24.3	3.2	334	15	23	89.3	99.8	2.2	2.3
N = 0%	5.5	5.5	7	39.9	5.6	25.5	3.2	437	18	25	86.8	99.7	2.6	2.3

Figure 20. Concentrations evolution of Co, Li, Ni and Na in the two stages pseudo-cc tests in the aqueous phase (a) and in the organic phase (b). 0.3 M Cyanex 272 in Isopar L, $\theta = 1$, T = 21 ± 2°C, t_{eq}=15 min. N = 45% indicates the test with saponified solvent, N = 0% indicates the test in which the pH was adjusted by NaOH addition to 5.5 ± 0.1. The values reported are averages of the last three iterations. Six total iterations were performed. Number of stages follows the flow of aqueous phase (left to right).

41

The similar results obtained in the two tests might however be a coincidence and further tests would be needed to gain a deeper knowledge of the extraction equilibria of the system with the saponified solvent. Pseudo-cc tests seem indeed necessary to gather accurate data on counter-current performances of SX systems with saponified solvents prior to pilot testing.

5.2.4   Summary

The results obtained in this work (Manuscript II) can be summarized as follows:

- Based on the phase behaviour of the solvent and its expected water content, using a higher (e.g., 10 M) concentration of NaOH for saponification seems to be advantageous. Using lower concentrations might however be beneficial in specific cases.
- Temperature does not impact the phase behaviour of the solvent here investigated but only its viscosity.
- The increase in the aqueous phase pH observed after contact with the saponified solvent can be caused both by a combination of chemical equilibria between the extractant (HA), its sodium salt (NaA) and the extracted metals, and by the rupture of the reverse micellar aggregates which release their aqueous core in the heavier phase.
- 95% of Co could be extracted from an NMC9.5.5 PLS using 45% saponified 0.3 M Cyanex 272 in Isopar L at pH = 5.5 ± 0.1 and $\theta = 1$.
- The McCabe-Thiele method showed to be inaccurate in predicting the extraction equilibria of a counter-current cascade when a saponified solvent is used. Pseudo-cc tests are necessary if accurate information on the extraction equilibria is needed before proceeding with pilot testing.
- 99.8% of Co was extracted in two stages using 45% saponified 0.3 M Cyanex 272 in Isopar L at $\theta = 1$ ($pH_{E1} = 5.4$, $pH_{E2} = 5.9$). The co-extraction of Ni and Li was about 2%. Similar results were obtained when the extraction was performed in two stages adjusting the pH at 5.5 ± 0.1 in both stages.

6 Conclusions

Considering the great volume of EOL LIBs which is expected to be available soon, developing efficient recycling processes is fundamental to minimize their environmental impact. SX is a well-established separation method which allows to efficiently recover high purity products and proved to be a promising solution for the separation and recovery of transition metals (Mn, Co, Ni) from NMC EOL LIBs. In this work, the use of SX to recover Mn and Co from such a waste was further investigated.

In the first study, the feasibility of recovering Mn as high purity $MnSO_4 \cdot H_2O$ from a purified NMC111 PLS combining SX and EC was investigated.

More than 98% of the Mn present in the feed was recovered and high purity ($99.6 \pm 0.1\%$) $MnSO_4 \cdot H_2O$ could be crystallized from the product obtained from a solvent extraction circuit composed of 3 extraction stages (35% v/v D2EHPA in Isopar L, pH = 2.9 ± 0.1, $\theta = 1$), 2 scrubbing stages (Mn = 4 g/L, $\theta = 1$) and 2 stripping stages ($H_2SO_4 = 0.5$ M, $\theta = 1$).

If D2EHPA is used for Mn extraction, Ca and Zn must be removed from the feed solution to avoid contamination of the final product. The presence of highly concentrated Na in the feed and the addition of NaOH resulted in the presence of traces of Na in the product. Al was partially extracted and could not be scrubbed or stripped from the organic phase. Mg was partially extracted, and traces could be found in the final product. Si was partially extracted but its measurement proved to be challenging due to its low concentration and the impossibility of obtaining a reliable measurement using ICP-MS. Assessing the impact of the presence of different impurities in the final product is challenging because of the lack of detailed information regarding the tolerated quantity of impurities both in the solution from which the pCAM is precipitated and the pCAM itself.

Finally, the presence of excess sulfuric acid in the stripping stage has shown to contribute to the formation of a liquid residue which contains H_2SO_4, traces of the solvent and traces of Mn which needs to be separated from the $MnSO_4 \cdot H_2O$ product. As the presence of solvent in such residue cannot be avoided (mutual miscibility), reducing the amount of excess acid used for stripping is important to minimize the volume of liquid that needs to be separated after crystallization.

In the second work, the extraction of Co by saponified Cyanex 272 was investigated with particular attention for gathering data which could guide in the choice of saponification conditions and for clarifying the behaviour of pre-neutralized solvents in counter-current extraction.

From the pseudo-ternary phase diagrams, it could be concluded that the degree of saponification (N), the concentration of NaOH and the Cyanex 272 content have an influence on the phase behaviour of the solvent. On the other hand, temperature had a negligible impact but might help in lowering the solvent viscosity in specific conditions. Using higher concentrations of NaOH seems to be advantageous for saponification as they minimize the amount of water added to the system but tend to stabilize the formation of microemulsions which might be disadvantageous if the water content of the solvent is high enough to affect the phase ratio of the SX system. In the latter case, lowering the concentration of NaOH might promote the formation of a biphasic system allowing for separation of the hydrophilic and hydrophobic layers.

Pseudo-cc tests showed that 99.8% of Co could be recovered in two stages using 45% saponified 0.3 M Cyanex 272, with about 2% co-extraction of Ni and Li. The pH in the two stages was respectively 5.4 and 5.9 ± 0.1. Similar overall extractions were obtained when the same solvent was contacted with the feed in two stages at pH = 5.5 ± 0.1. However, the McCabe-Thiele method was shown to be inaccurate in predicting multistage extraction equilibria when a saponified solvent is used. Pseudo-cc tests are in this case required to obtain accurate equilibrium data for a counter-current cascade making the prediction of multi-stage equilibrium challenging.

7   Future work

In this work, the extraction of Mn and Co was performed using D2EHPA and Cyanex 272 following the strategy in which the transition metals are separated in three high purity streams to be used for the synthesis of new CAM. The stringent purity requirements on the products obtained with such approach (Figure 2a, Page 9) result in a complex process which involves multiple stages of extraction, scrubbing and stripping for each metal. Moreover, efficient recirculation of the products/raffinates must be implemented to avoid the presence of open loops and minimize the secondary waste production, making the optimization of the SX flowsheet challenging. Future work should focus on the development of simpler processes aimed at minimizing the number of operations involved, reducing the presence of streams that need to be recirculated and diminishing the solvent consumption. Separation of the transition metals in different streams should however still be achieved to allow flexibility in the production of the CAM.

As many different NMC LIBs chemistries are nowadays available on the market, the development of a SX process should be sided by a study in which its flexibility towards the feed composition is assessed. Understanding how fluctuations in the composition of the feed material affect the SX process and developing suitable measures to mitigate such variations is fundamental to ensure the feasibility of the process. Moreover, depending on the operations performed upstream of SX and the different NMC chemistries different cationic and anionic impurities might be present in the feed solution. Investigating the distribution of such impurities and their impact on the extraction would benefit the development of future processes.

Acknowledgments

I would like to express my gratitude to my supervisor Martina Petranikova for her guidance, her trust and the patience she had during this time. I am also grateful to Burcak Ebin and Christian Ekberg that alternated as my co-supervisors. Many thanks also to Amit and Ilyes for their valuable feedbacks and support. I am thankful to Romain Bordes for finding the time to help me with the chemistry of surfactants. I would also like to thank Teodora Retegan Vollmer and Mark Foreman for their help and for welcoming me in my first experience here at Chalmers.

Many thanks to Léa, Nils, and Alejandro that made feel at home from the moment I arrived in Sweden. Thanks also to my two great officemates Thomas and Simon, to all the friends and colleagues at NC/IMR and to the students I had the pleasure of working with. Special thanks to Maja and Camille.

Finally, huge thanks to my family and friends for all their love and support.

Bibliography

1. Latini, D.; Vaccari, M.; Lagnoni, M.; Orefice, M.; Mathieux, F.; Huisman, J.; Tognotti, L.; Bertei, A. A Comprehensive Review and Classification of Unit Operations with Assessment of Outputs Quality in Lithium-Ion Battery Recycling. *J Power Sources* 2022, *546*.

2. Ritchie, H.; Rosado, P.; Roser, M. CO_2 and Greenhouse Gas Emissions.

3. Ritchie, H.; Rosado, P.; Roser, M. Breakdown of Carbon Dioxide, Methane and Nitrous Oxide Emissions by Sector.

4. Ritchie, H. Cars, Planes, Trains: Where Do CO_2 Emissions from Transport Come From?

5. Energy Agency, I. *Global EV Outlook 2024 Moving towards Increased Affordability*; 2024;

6. Fleischmann, J.; Hanicke, M.; Horetsky, E.; Ibrahim, D.; Jautelat, S.; Linder, M.; Schaufuss, P.; Torscht, L.; Rijt, A. Van De Battery 2030: Resilient, Sustainable, and Circular. Battery Demand Is Growing — and so Is the Need For. *McKinsey & Company* 2023.

7. Carrara, S..; Bobba, S..; Blagoeva, D..; Alves Dias, P..; Cavalli, A..; Georgitzikis, K..; Grohol, M..; Itul, A..; Kuzov, T..; Latunussa, C..; et al. *Supply Chain Analysis and Material Demand Forecast in Strategic Technologies and Sectors in the EU : A Foresight Study*; Publications Office of the European Union, 2023; ISBN 9789268003398.

8. Business Sweden The Nordic Battery Value Chain. **2023**.

9. European Union Critical Raw Materials Act.

10. European Commission *Study on the Critical Raw Materials for the EU 2023 Final Report*; 2023; ISBN 9789268004135.

11. Neumann, J.; Petranikova, M.; Meeus, M.; Gamarra, J.D.; Younesi, R.; Winter, M.; Nowak, S. Recycling of Lithium-Ion Batteries-Current State of the Art, Circular Economy, and Next Generation Recycling. **2022**, doi:10.1002/aenm.202102917.

12. European Commission Regulation (EU) 2023/1542 of the European Parliament and of the Council Concerning Batteries and Waste Batteries. *European Commission* 2023, *2023*, 1–117.

13. Velázquez-Martínez, O.; Valio, J.; Santasalo-Aarnio, A.; Reuter, M.; Serna-Guerrero, R. A Critical Review of Lithium-Ion Battery Recycling Processes from a Circular Economy Perspective. *Batteries* 2019, *5*.

14. N. Jantunen, S. Virolainen, T.S. Direct Production of Ni – Co – Mn Mixtures for Cathode Precursors from Cobalt-Rich Lithium-Ion Battery Leachates by Solvent Extraction. *Metals (Basel)* **2022**, *12*, doi:https://doi.org/10.3390/ met12091445.

15. Winslow, K.M.; Laux, S.J.; Townsend, T.G. A Review on the Growing Concern and Potential Management Strategies of Waste Lithium-Ion Batteries. *Resour Conserv Recycl* 2018, *129*, 263–277.

16. Windisch-Kern, S.; Gerold, E.; Nigl, T.; Jandric, A.; Altendorfer, M.; Rutrecht, B.; Scherhaufer, S.; Raupenstrauch, H.; Pomberger, R.; Antrekowitsch, H.; et al. Recycling Chains for Lithium-Ion Batteries: A Critical Examination of Current Challenges, Opportunities and Process Dependencies. *Waste Management* 2022, *138*, 125–139.

17. Heelan, J.; Gratz, E.; Zheng, Z.; Wang, Q.; Chen, M.; Apelian, D.; Wang, Y. Current and Prospective Li-Ion Battery Recycling and Recovery Processes. *JOM* 2016, *68*, 2632–2638.

18. Harper, G.D.J.; Kendrick, E.; Anderson, P.A.; Mrozik, W.; Christensen, P.; Lambert, S.; Greenwood, D.; Das, P.K.; Ahmeid, M.; Milojevic, Z.; et al. Roadmap for a Sustainable Circular Economy in Lithium-Ion and Future Battery Technologies. *JPhys Energy* **2023**, *5*, doi:10.1088/2515-7655/acaa57.

19. Malik, M.; Chan, K.H.; Azimi, G. Review on the Synthesis of LiNixMnyCo1-x-YO2 (NMC) Cathodes for Lithium-Ion Batteries. *Mater Today Energy* 2022, *28*.

20. Meshram, P.; Mishra, A.; Abhilash; Sahu, R. Environmental Impact of Spent Lithium Ion Batteries and Green Recycling Perspectives by Organic Acids – A Review. *Chemosphere* 2020, *242*.

21. Manthiram, A. A Reflection on Lithium-Ion Battery Cathode Chemistry. *Nat Commun* 2020, *11*.

22. Ryu, H.H.; Sun, H.H.; Myung, S.T.; Yoon, C.S.; Sun, Y.K. Reducing Cobalt from Lithium-Ion Batteries for the Electric Vehicle Era. *Energy Environ Sci* 2021, *14*, 844–852.

23. Lee, S.; Manthiram, A. Can Cobalt Be Eliminated from Lithium-Ion Batteries? *ACS Energy Lett* **2022**, 3058–3063, doi:10.1021/acsenergylett.2c01553.

24. Sun, X.; Hao, H.; Liu, Z.; Zhao, F. Insights into the Global Flow Pattern of Manganese. *Resources Policy* **2020**, *65*, doi:10.1016/j.resourpol.2019.101578.

25. Cannon, W.F.; Kimball, B.E.; Corathers, L.A. *Critical Mineral Resources of the United States—Economic and Environmental Geology and Prospects for Future Supply*; Reston, Virginia, 2017;

26. Our World in Data Manganese Production, 1900 to 2023.

27. Global Manganese Production by Country 2021 | Statista Available online: https://www.statista.com/statistics/1244066/global-manganese-production-volume-by-country/ (accessed on 13 March 2024).

28. Manganese Available online: https://giyanimetals.com/manganese (accessed on 13 March 2024).

29. Chandra, M.; Yu, D.; Tian, Q.; Guo, X. Recovery of Cobalt from Secondary Resources: A Comprehensive Review. *Mineral Processing and Extractive Metallurgy Review* **2022**, *43*, 679–700, doi:10.1080/08827508.2021.1916927.

30. Our World in Data Cobalt Production-Reserves.

31.   Our World in Data Nickel Production, 1900 to 2023.

32.   Larouche, F.; Tedjar, F.; Amouzegar, K.; Houlachi, G.; Bouchard, P.; Demopoulos, G.P.; Zaghib, K. Progress and Status of Hydrometallurgical and Direct Recycling of Li-Ion Batteries and Beyond. *Materials* 2020, *13*.

33.   Ali, H.; Khan, H.A.; Pecht, M.G. Circular Economy of Li Batteries: Technologies and Trends. *J Energy Storage* 2021, *40*.

34.   Mossali, E.; Picone, N.; Gentilini, L.; Rodrìguez, O.; Pérez, J.M.; Colledani, M. Lithium-Ion Batteries towards Circular Economy: A Literature Review of Opportunities and Issues of Recycling Treatments. *J Environ Manage* **2020**, *264*, doi:10.1016/j.jenvman.2020.110500.

35.   Werner, D.; Peuker, U.A.; Mütze, T. Recycling Chain for Spent Lithium-ion Batteries. *Metals (Basel)* **2020**, *10*, doi:10.3390/met10030316.

36.   Barbosa de Mattos, D.F.; Duda, S.; Petranikova, M. Recycling of Lithium Iron Phosphate (LiFePO4) Batteries from the End Product Quality Perspective. *Batteries* 2025, *11*.

37.   Hayagan, N.; Aymonier, C.; Croguennec, L.; Morcrette, M.; Dedryvère, R.; Olchowka, J.; Philippot, G. A Holistic Review on the Direct Recycling of Lithium-Ion Batteries from Electrolytes to Electrodes. *J Mater Chem A Mater* 2024.

38.   Zhang, J. Pyrometallurgy-Based Applications in Spent Lithium-Ion Battery Recycling. In *Nano Technology for Battery Recycling, Remanufacturing, and Reusing*; Elsevier, 2022; pp. 171–182 ISBN 9780323911344.

39.   Cornelio, A.; Zanoletti, A.; Bontempi, E. Recent Progress in Pyrometallurgy for the Recovery of Spent Lithium-Ion Batteries: A Review of State-of-the-Art Developments. *Curr Opin Green Sustain Chem* 2024, *46*.

40.   Li, P.; Luo, S.; Zhang, L.; Liu, Q.; Wang, Y.; Lin, Y.; Xu, C.; Guo, J.; Cheali, P.; Xia, X. Progress, Challenges, and Prospects of Spent Lithium-Ion Batteries Recycling: A Review. *Journal of Energy Chemistry* 2024, *89*, 144–171.

41.   Piątek, J.; Afyon, S.; Budnyak, T.M.; Budnyk, S.; Sipponen, M.H.; Slabon, A. Sustainable Li-Ion Batteries: Chemistry and Recycling. *Adv Energy Mater* **2021**, *11*, doi:10.1002/aenm.202003456.

42.   Vieceli, N.; Benjamasutin, P.; Promphan, R.; Hellström, P.; Paulsson, M.; Petranikova, M. Recycling of Lithium-Ion Batteries: Effect of Hydrogen Peroxide and a Dosing Method on the Leaching of LCO, NMC Oxides, and Industrial Black Mass. *ACS Sustain Chem Eng* **2023**, *11*, 9662–9673, doi:10.1021/ACSSUSCHEMENG.3C01238.

43.   Vieceli, N.; Benjamasutin, P.; Promphan, R.; Hellström, P.; Paulsson, M.; Petranikova, M. Recycling of Lithium-Ion Batteries: Effect of Hydrogen Peroxide on the Leaching of Lco, Nmc Oxides, and Black Mass. *SSRN Electronic Journal* **2022**, doi:10.2139/SSRN.4157169.

44. Gerold, E.; Schinnerl, C.; Antrekowitsch, H. Critical Evaluation of the Potential of Organic Acids for the Environmentally Friendly Recycling of Spent Lithium-Ion Batteries. *Recycling* **2022**, *7*, doi:10.3390/recycling7010004.

45. Golmohammadzadeh, R.; Faraji, F.; Rashchi, F. Recovery of Lithium and Cobalt from Spent Lithium Ion Batteries (LIBs) Using Organic Acids as Leaching Reagents: A Review. *Resour Conserv Recycl* 2018, *136*, 418–435.

46. Rouquette, L.M.J.; Petranikova, M.; Vieceli, N. Complete and Selective Recovery of Lithium from EV Lithium-Ion Batteries: Modeling and Optimization Using Oxalic Acid as a Leaching Agent. *Sep Purif Technol* **2023**, *320*, doi:10.1016/j.seppur.2023.124143.

47. Klaehn, J.R.; Shi, M.; Diaz, L.A.; Molina, D.E.; Reich, S.M.; Palasyuk, O.; Repukaiti, R.; Lister, T.E. Removal of Impurity Metals as Phosphates from Lithium-Ion Battery Leachates. *Hydrometallurgy* **2023**, *217*, doi:10.1016/j.hydromet.2023.106041.

48. Chernyaev, A.; Wilson, B.P.; Lundström, M. Study on Valuable Metal Incorporation in the Fe-Al Precipitate during Neutralization of LIB Leach Solution. *Scientific Reports |* **123AD**, *11*, 23283, doi:10.1038/s41598-021-02019-2.

49. Chernyaev, A.; Zhang, J.; Seisko, S.; Louhi-Kultanen, M.; Lundström, M. Fe 3+ and Al 3+ Removal by Phosphate and Hydroxide Precipitation from Synthetic NMC Li-Ion Battery Leach Solution. *Scientific Reports |* **123AD**, *13*, 21445, doi:10.1038/s41598-023-48247-6.

50. Virolainen, S.; Wesselborg, T.; Kaukinen, A.; Sainio, T. Removal of Iron, Aluminium, Manganese and Copper from Leach Solutions of Lithium-Ion Battery Waste Using Ion Exchange. *Hydrometallurgy* **2021**, *202*, doi:10.1016/j.hydromet.2021.105602.

51. Nozari, I.; Azizi, A. An Investigation into the Extraction Behavior of Copper from Sulfate Leach Liquor Using Acorga M5640 Extractant: Mechanism, Equilibrium, and Thermodynamics., doi:10.1007/s42461-020-00280-z/Published.

52. Tsakiridis, P.E.; Agatzini-Leonardou, S. Solvent Extraction of Aluminium in the Presence of Cobalt, Nickel and Magnesium from Sulphate Solutions by Cyanex 272. *Hydrometallurgy* **2005**, *80*, 90–97, doi:10.1016/j.hydromet.2005.07.002.

53. Tan, J.; Wang, Q.; Chen, S.; Li, Z.; Sun, J.; Liu, W.; Yang, W.; Xiang, X.; Sun, X.; Duan, X. Recycling-Oriented Cathode Materials Design for Lithium-Ion Batteries: Elegant Structures versus Complicated Compositions. *Energy Storage Mater* **2021**, *41*, 380–394, doi:10.1016/J.ENSM.2021.06.021.

54. Jung, J.; Sui, P.-C.; Zhang, J. *Hydrometallurgical Recycling of Lithium-Ion Battery Materials*;

55. Ma, Y.; Svärd, M.; Xiao, X.; Gardner, J.M.; Olsson, R.T.; Forsberg, K. Precipitation and Crystallization Used in the Production of Metal Salts for Li-Ion Battery Materials: A Review. *Metals (Basel)* **2020**, *10*, 1–16, doi:10.3390/met10121609.

56. Wesselborg, T.; Asumalahti, S.; Virolainen, S.; Sainio, T. Continuous Multicolumn Ion Exchange Process for Spent Lithium-Ion Battery Leachate: Recovery and Purification of a Li+Ni+Co Mixture. *Sep Purif Technol* **2025**, *353*, doi:10.1016/j.seppur.2024.128351.

57. Strauss, M.L.; Diaz, L.A.; McNally, J.; Klaehn, J.; Lister, T.E. Separation of Cobalt, Nickel, and Manganese in Leach Solutions of Waste Lithium-Ion Batteries Using Dowex M4195 Ion Exchange Resin. *Hydrometallurgy* **2021**, *206*, doi:10.1016/j.hydromet.2021.105757.

58. Wesselborg, T.; Virolainen, S.; Sainio, T. Recovery of Lithium from Leach Solutions of Battery Waste Using Direct Solvent Extraction with TBP and FeCl3. *Hydrometallurgy* **2021**, *202*, 105593, doi:10.1016/j.hydromet.2021.105593.

59. Lei, S.; Sun, W.; Yang, Y. Solvent Extraction for Recycling of Spent Lithium-Ion Batteries. *J Hazard Mater* **2022**, *424*.

60. Zhang, W.; Cheng, C.Y. Manganese Metallurgy Review. Part II: Manganese Separation and Recovery from Solution. *Hydrometallurgy* **2007**, *89*, 160–177, doi:10.1016/J.HYDROMET.2007.08.009.

61. Flett, D.S. Cobalt-Nickel Separation in Hydrometallurgy: A Review. *Chemistry for Sustainable Development* **2004**, *12*, 81–91.

62. Devi, N.B.; Nathsarma, K.C.; Chakravortty, V. Separation and Recovery of Cobalt(II) and Nickel(II) from Sulphate Solutions Using Sodium Salts of D2EHPA, PC 88A and Cyanex 272. *Hydrometallurgy* **1998**, *49*, 47–61, doi:10.1016/S0304-386X(97)00073-X.

63. Omelchuk, K.; Szczepański, P.; Shrotre, A.; Haddad, M.; Chagnes, A. Effects of Structural Changes of New Organophosphorus Cationic Exchangers on a Solvent Extraction of Cobalt, Nickel and Manganese from Acidic Chloride Media. *RSC Adv* **2017**, *7*, 5660–5668, doi:10.1039/c6ra21695a.

64. Vieceli, N.; Reinhardt, N.; Ekberg, C.; Petranikova, M. Optimization of Manganese Recovery from a Solution Based on Lithium-Ion Batteries by Solvent Extraction with D2ehpa. *Metals (Basel)* **2021**, *11*, doi:10.3390/met11010054.

65. Vieceli, N.; Vonderstein, C.; Swiontek, T.; Stopic, S.; Dertmann, C.; Sojka, R.; Reinhardt, N.; Ekberg, C.; Friedrich, B.; Petranikova, M. Recycling of Li-Ion Batteries from Industrial Processing: Uspscaled Hydrometallurgical Treatment and Recovery of High Purity Manganese by Solvent Extraction. *Solvent Extraction and Ion Exchange* **2023**, *41*, 205–220, doi:https://doi.org/10.1080/07366299.2023.2165405.

66. Keller, A.; Hlawitschka, M.W.; Bart, H.J. Application of Saponified D2EHPA for the Selective Extraction of Manganese from Spend Lithium-Ion Batteries. *Chemical Engineering and Processing - Process Intensification* **2022**, *171*, 108552, doi:10.1016/J.CEP.2021.108552.

67. Keller, A.; Hlawitschka, M.W.; Bart, H.J. Manganese Recycling of Spent Lithium Ion Batteries via Solvent Extraction. *Sep Purif Technol* **2021**, *275*, doi:10.1016/J.SEPPUR.2021.119166.

68. Chen, X.; Chen, Y.; Zhou, T.; Liu, D.; Hu, H.; Fan, S. Hydrometallurgical Recovery of Metal Values from Sulfuric Acid Leaching Liquor of Spent Lithium-Ion Batteries. *Waste Management* **2015**, *38*, 349–356, doi:10.1016/j.wasman.2014.12.023.

69. Tang, Y.C.; Wang, J.Z.; Shen, Y.H. Separation of Valuable Metals in The Recycling of Lithium Batteries via Solvent Extraction. *Minerals* **2023**, *13*, doi:10.3390/min13020285.

70.   Vieceli, N.; Ottink, T.; Stopic, S.; Dertmann, C.; Swiontek, T.; Vonderstein, C.; Sojka, R.; Reinhardt, N.; Ekberg, C.; Friedrich, B.; et al. Solvent Extraction of Cobalt from Spent Lithium-Ion Batteries: Dynamic Optimization of the Number of Extraction Stages Using Factorial Design of Experiments and Response Surface Methodology. *Sep Purif Technol* **2023**, *307*, doi:10.1016/j.seppur.2022.122793.

71.   Reddy, B.R.; Park, K.H. Process for the Recovery of Cobalt and Nickel from Sulphate Leach Liquors with Saponified Cyanex 272 and D2EHPA. *Sep Sci Technol* **2007**, *42*, 2067–2080, doi:10.1080/01496390701310496.

72.   Park, K.H.; Mohapatra, D. Process for Cobalt Separation and Recovery in the Presence of Nickel from Sulphate Solutions by Cyanex 272. *Metals and Materials International* **2006**, *12*, 441–446, doi:10.1007/BF03027712/METRICS.

73.   Rodrigues, I.R.; Deferm, C.; Binnemans, K.; Riaño, S. Separation of Cobalt and Nickel via Solvent Extraction with Cyanex-272: Batch Experiments and Comparison of Mixer-Settlers and an Agitated Column as Contactors for Continuous Counter-Current Extraction. *Sep Purif Technol* **2022**, *296*, doi:10.1016/j.seppur.2022.121326.

74.   Parween, R.; Rani, K.; Panda, R.; Sharma, A.; Ambade, B.; Kumar Jha, M. Hydrometallurgical Separation and Purification to Recover Iron (Fe), Copper (Cu), Nickel (Ni), Lithium (Li), Cobalt (Co), and Manganese (Mn) Metals from the Leach Liquor of Discarded LIBs. *Sep Purif Technol* **2025**, *364*, doi:10.1016/j.seppur.2025.132325.

75.   Liu, W.; Zhang, J.; Xu, Z.; Liang, J.; Zhu, Z. Study on the Extraction and Separation of Zinc, Cobalt, and Nickel Using Ionquest 801, Cyanex 272, and Their Mixtures. *Metals (Basel)* **2021**, *11*, 1–12, doi:10.3390/met11030401.

76.   Yang, Y.; Lei, S.; Song, S.; Sun, W.; Wang, L. Stepwise Recycling of Valuable Metals from Ni-Rich Cathode Material of Spent Lithium-Ion Batteries. *Waste Management* **2020**, *102*, 131–138, doi:10.1016/J.WASMAN.2019.09.044.

77.   Chen, W.S.; Ho, H.J. Recovery of Valuable Metals from Lithium-Ion Batteries NMC Cathode Waste Materials by Hydrometallurgical Methods. *Metals 2018, Vol. 8, Page 321* **2018**, *8*, 321, doi:10.3390/MET8050321.

78.   Virolainen, S.; Fallah Fini, M.; Laitinen, A.; Sainio, T. Solvent Extraction Fractionation of Li-Ion Battery Leachate Containing Li, Ni, and Co. *Sep Purif Technol* **2017**, *179*, 274–282, doi:10.1016/j.seppur.2017.02.010.

79.   Yang, Y.; Xu, S.; He, Y. Lithium Recycling and Cathode Material Regeneration from Acid Leach Liquor of Spent Lithium-Ion Battery via Facile Co-Extraction and Co-Precipitation Processes. *Waste Management* **2017**, *64*, 219–227, doi:10.1016/J.WASMAN.2017.03.018.

80.   Shuya, L.; Yang, C.; Xuefeng, C.; Wei, S.; Yaqing, W.; Yue, Y. Separation of Lithium and Transition Metals from Leachate of Spent Lithium-Ion Batteries by Solvent Extraction Method with Versatic 10. *Sep Purif Technol* **2020**, *250*, doi:10.1016/j.seppur.2020.117258.

81.   Lin, X.; Liu, G.; Wang, X.; Wu, M.; Chang, N. Lithium-Ion Battery Recycling Technologies towards Sustainable Electric Vehicle Industry. **2023**, 1–9.

82. Kang, J.; Senanayake, G.; Sohn, J.; Shin, S.M. Recovery of Cobalt Sulfate from Spent Lithium Ion Batteries by Reductive Leaching and Solvent Extraction with Cyanex 272. *Hydrometallurgy* **2010**, *100*, 168–171, doi:10.1016/J.HYDROMET.2009.10.010.

83. Sattar, R.; Ilyas, S.; Bhatti, H.N.; Ghaffar, A. Resource Recovery of Critically-Rare Metals by Hydrometallurgical Recycling of Spent Lithium Ion Batteries. *Sep Purif Technol* **2019**, *209*, 725–733, doi:10.1016/j.seppur.2018.09.019.

84. Rydberg, J.; Cox, M.; Musikas, C.; Choppin, G.R. Solvent Extraction Principles and Practice. In; 2004 ISBN 0824750632.

85. V. S. Kislik *Solvent Extraction: Classical and Novel Approaches*; First.; Elsevier, 2012; ISBN 9780444537782.

86. Ritcey, G.M.; Ashbrook, A.W. *Solvent Extraction Principles and Applications to Process Metallurgy*; First.; Elsevier, 1984; Vol. 1;.

87. Solomon, T. *The Definition and Unit of Ionic Strength*; 2001; Vol. 78;.

88. Reed, D.T.; Clark, S.B.; Rao, L. *Actinide Speciation in High Ionic Strength Media*; Springer US, 1999;

89. Pitzer, K.S.. *Activity Coefficients in Electrolyte Solutions*; CRC Press, 1991; ISBN 0849354153.

90. Separation Factor. **2025**, doi:doi:10.1351/goldbook.S05615.

91. Fu, X.; Hu, Z.; Liu, Y.; Golding, J.A. Extraction of Sodium in Bis (2, 4,4 - Trimethylpentyl) Phosphinic Acid "Cyanex 272"Tm: Basic Constants and Extraction Equilibria. *Solvent Extraction and Ion Exchange* **1990**, *8*, 573–595, doi:10.1080/07366299008918018.

92. Geng, P.; Wang, X. Determination of Some Basic Constants for HDEHP and the Equilibrium Constants for Its Extraction of Trivalent Light Rare Earth Ions. *J. Beijing Univ.* **1982**, *5*.

93. Paatero, E.; Sjöblom, J. Phase Behaviour in Metal Extraction Systems. *Hydrometallurgy* **1990**, *25*, 231–256, doi:10.1016/0304-386X(90)90041-Y.

94. El Maangar, A.; Lopian, T.; Dourdain, S.; Kunz, W.; Zemb, T. Diluent Effects on the Stability Range of w/o Micellar Systems and Microemulsions Made with Anionic Extractants. *EPJ Nuclear Sci. Technol.* **2022**, *8*, doi:https://doi.org/10.1051/epjn/2022025.

95. Kronberg, B.; Holmberg, K.; Lindman, B. *Surface Chemistry of Surfactants and Polymers*; Wiley, 2017;

96. Ritcey, G.M.; Ashbrook, A.W. *Solvent Extraction Principles and Applications to Process Metallurgy*; Elsevier, 1984; Vol. 2;.

97. Paatero, E. The Effects of Amphiphilic Aggregation and Phase Equilibria on Metal Extraction Processes, Åbo Akademi: Åbo, 1990.

98. Paatero, E.; Lantto, T.; Ernola, P. The Effect of Trioctylphosphine Oxide on Phase and Extraction Equilibria in Systems Containing Bis(2,4,4-Trimethylpentyl)Phosphinic Acid. *Solvent Extraction and Ion Exchange* **1990**, *8*, 371–388, doi:10.1080/07366299008918006.

99. Paatero, E.; Ernola, P.; Sjöblom, J.; Hummelstedt, L. Formation of Microemulsions in Solvent Extraction Systems Containing Cyanex 272. In Proceedings of the Proceedings of the International Solvent Extraction Conference (ISEC'88); USSR Academy of Sciences: Moscow, 1988; pp. 124–127.

100. Zhou, N.; Wu, J. Review on Aggregation of Acid Extractants in Solvent Extraction of Metal Ions: Remark on the General Model*. *Progress in Natural Science* **2003**, *13*, 1–12, doi:10.1080/10020070312331343050.

101. Cheng, C.Y. Purification of Synthetic Laterite Leach Solution by Solvent Extraction Using D2EHPA. *Hydrometallurgy* **2000**, *56*, 369–386, doi:10.1016/S0304-386X(00)00095-5.

102. Grymonprez, B.; Lommelen, R.; Bussé, J.; Binnemans, K.; Riaño, S. Solubility of Di-(2-Ethylhexyl)Phosphoric Acid (D2EHPA) in Aqueous Electrolyte Solutions: Studies Relevant to Liquid-Liquid Extraction. *Sep Purif Technol* **2024**, *333*, 125846, doi:10.1016/J.SEPPUR.2023.125846.

103. Lee, P.C.; Li, C.W.; Chen, J.Y.; Li, Y.S.; Chen, S.S. Dissolution of D2EHPA in Liquid-Liquid Extraction Process: Implication on Metal Removal and Organic Content of the Treated Water. *Water Res* **2011**, *45*, 5953–5958, doi:10.1016/j.watres.2011.08.054.

104. Schmitt, J.M.; Blake Jr., C.A. *Purification of Di(2-Ethylhexyl)Phosphoric Acid*; Oak Ridge, Tennessee, 1964;

105. Nasser, O.A.; Petranikova, M. Review of Achieved Purities after Li-Ion Batteries Hydrometallurgical Treatment and Impurities Effects on the Cathode Performance. *Batteries* **2021**, *7*, doi:10.3390/batteries7030060.

106. Peng, C.; Chang, C.; Wang, Z.; Wilson, B.P.; Liu, F.; Lundstro, M. CLEANER MANUFACTURING OF CRITICAL METALS Recovery of High-Purity MnO 2 from the Acid Leaching Solution of Spent Li-Ion Batteries. *JOM* **2020**, *72*, doi:10.1007/s11837-019-03785-1.

107. Reuna, S.; Väisänen, A. Purification of Recovered Phosphoric Acid by Extracting Aluminium with Di-2-Ethylhexyl Phosphoric Acid. *Chemical Papers* **2022**, *76*, 417–425, doi:10.1007/s11696-021-01848-9.

108. Mohapatra, D.; Hong-In, K.; Nam, C.W.; Park, K.H. Liquid-Liquid Extraction of Aluminium(III) from Mixed Sulphate Solutions Using Sodium Salts of Cyanex 272 and D2EHPA. *Sep Purif Technol* **2007**, *56*, 311–318, doi:10.1016/j.seppur.2007.02.017.

109. Di-(2-Ethylhexyl)Phosphoric Acid | C16H35O4P | ChemSpider Available online: http://www.chemspider.com/Chemical-Structure.8918.html (accessed on 17 March 2024).

110. Mono-(2-Ethylhexyl)-Phosphoric Acid CAS#: 14660-16-3 Available online: https://www.chemicalbook.com/ProductChemicalPropertiesCB14634437_EN.htm (accessed on 17 March 2024).

111. Tris(2-Ethylhexyl) Phosphate | 78-42-2 Available online: https://www.chemicalbook.com/ChemicalProductProperty_EN_CB4670674.htm (accessed on 17 March 2024).

112. 2-ETHYL HEXANOL | CAMEO Chemicals | NOAA Available online: https://cameochemicals.noaa.gov/chemical/8639 (accessed on 17 March 2024).

113. Kauppinen, T.; Laine, P.; Välikangas, J.; Tynjälä, P.; Hu, T.; Salminen, J.; Lassi, U. Co-Precipitation of NCM 811 Using Recycled and Purified Manganese: Effect of Impurities on the Battery Cell Performance. *ChemElectroChem* **2023**, *10*, doi:10.1002/celc.202300265.

114. Chen, M.; Zhao, E.; Chen, D.; Wu, M.; Han, S.; Huang, Q.; Yang, L.; Xiao, X.; Hu, Z. Decreasing Li/Ni Disorder and Improving the Electrochemical Performances of Ni-Rich LiNi0.8Co0.1Mn0.1O2 by Ca Doping. *Inorg Chem* **2017**, *56*, 8355–8362, doi:10.1021/ACS.INORGCHEM.7B01035/ASSET/IMAGES/LARGE/IC-2017-010356_0006.JPEG.

115. Zhang, R.; Zheng, Y.; Yao, Z.; Vanaphuti, P.; Ma, X.; Bong, S.; Chen, M.; Liu, Y.; Cheng, F.; Yang, Z.; et al. Systematic Study of Al Impurity for NCM622 Cathode Materials. *ACS Sustain Chem Eng* **2020**, *8*, 9875–9884, doi:10.1021/ACSSUSCHEMENG.0C02965/ASSET/IMAGES/LARGE/SC0C02965_0005.JPEG.

116. Wu, T.; Wang, G.; Liu, B.; Huang, Q.; Su, Y.; Wu, F.; Kelly, R.M. The Role of Cu Impurity on the Structure and Electrochemical Performance of Ni-Rich Cathode Material for Lithium-Ion Batteries. *J Power Sources* **2021**, *494*, doi:10.1016/j.jpowsour.2021.229774.

117. Aleksovska, S.; Petrus Ïevski, V.M.; AE optrajanov, B.S. Calculation of Structural Parameters in Isostructural Series: The Kieserite Group. *International Union of Crystallography Acta Crystallographica Section B Acta Cryst* **1998**, *54*, 564–567.

118. Lindell, E.; Jaaskelainen, E.; Paatero, E.; Nyman, B.; ″″″″″ *Effect of Reversed Micelles in Co/Ni Separation by Cyanex 272*; 2000; Vol. 56;.

119. Jantunen, N.; Kauppinen, T.; Salminen, J.; Virolainen, S.; Lassi, U.; Sainio, T. Separation of Zinc and Iron from Secondary Manganese Sulfate Leachate by Solvent Extraction. *Miner Eng* **2021**, *173*, 107200, doi:10.1016/J.MINENG.2021.107200.

120. Biswas, R.K.; Habib, M.A.; Singha, H.P. Colorimetric Estimation and Some Physicochemical Properties of Purified Cyanex 272. *Hydrometallurgy* **2005**, *76*, 97–104, doi:10.1016/j.hydromet.2004.09.005.

121. Omelchuk, K.; Chagnes, A. New Cationic Exchangers for the Recovery of Cobalt(II), Nickel(II) and Manganese(II) from Acidic Chloride Solutions: Modelling of Extraction Curves. *Hydrometallurgy* **2018**, *180*, 96–103, doi:10.1016/j.hydromet.2018.07.003.

122. Kolarik, Z. Review: Dissociation, Self-Association, and Partition of Monoacidic Organophosphorus Extractants. *Solvent Extraction and Ion Exchange* **2010**, *28*, 707–763, doi:10.1080/07366299.2010.515172.

123. Fomina, P.S.; Proskurnin, M.A.; Mizaikoff, B.; Volkov, D.S. Infrared Spectroscopy in Aqueous Solutions: Capabilities and Challenges. *Crit Rev Anal Chem* 2023, *53*, 1748–1765.

124. Sun, M.; Liu, S.; Zhang, Y.; Liu, M.; Yi, X.; Hu, J. Insights into the Saponification Process of Di(2-Ethylhexyl) Phosphoric Acid Extractant: Thermodynamics and Structural Aspects. *J Mol Liq* **2019**, *280*, 252–258, doi:10.1016/j.molliq.2019.02.025.

125. İnan, S.; Tel, H.; Sert; Çetinkaya, B.; Sengül, S.; Özkan, B.; Altaş, Y. Extraction and Separation Studies of Rare Earth Elements Using Cyanex 272 Impregnated Amberlite XAD-7 Resin. *Hydrometallurgy* **2018**, *181*, 156–163, doi:10.1016/j.hydromet.2018.09.005.

126. Svend, E.; Rasmussen, J.-E.; Lundtoft, B. *Structures and Phase Transitions of Na2SO4*; 1996; Vol. 29;.

127. Fischmeister, H. The System Na2SO4-Na2CrO4 and the Structure of Na2SO4 (III). *Acta Cryst.* **1954**, *7*, 776.

Appendix A

Table A1. Concentration of the main elements contained in the NMC111 PLS after Mn extraction (Paper I). Values for which uncertainty are reported are averages of 3 measurements. pH = 2.8 ± 0.1, I = 5.8 M, E = 423 mV.

	Co	Ni	Li	Mn	Na	SO_4^{2-}	P
C (g/L)	9.75 ± 0.04	6.21 ± 0.02	3.74 ± 0.07	0.22 ± 0.01	59.9 ± 0.56	58.7 ± 0.1	0.07 ± 0.00
C (mM)	165 ± 1	106 ± 1	531 ± 2	4 ± 0	2607 ± 24	1831 ± 4	2 ± 0

Extraction of Co from the NMC111 feed solution after Mn removal was attempted using 0.85 M Cyanex 272 in Isopar L. Precipitation of a Na_2SO_4 (Figure A1) was observed at pH between 6.0-6.3 when a saponified solvent was used. The same phenomenon was observed at pH below 5 when NaOH 5 or 10 M was added to the system during the extraction. The lower pH at which Na_2SO_4 precipitates when NaOH is directly added to the system might be a consequence of local supersaturation around the NaOH drops. As the extraction of Co by Cyanex 272 would be carried out at pH around 5-5.5, no further investigation was carried out on this feed. To be able to perform Co extraction using Cyanex 272, a lower concentration of Na in the feed is needed. The pre-treatment stages, particularly the removal of impurities (Cu, Al, Fe), must be accordingly adjusted.
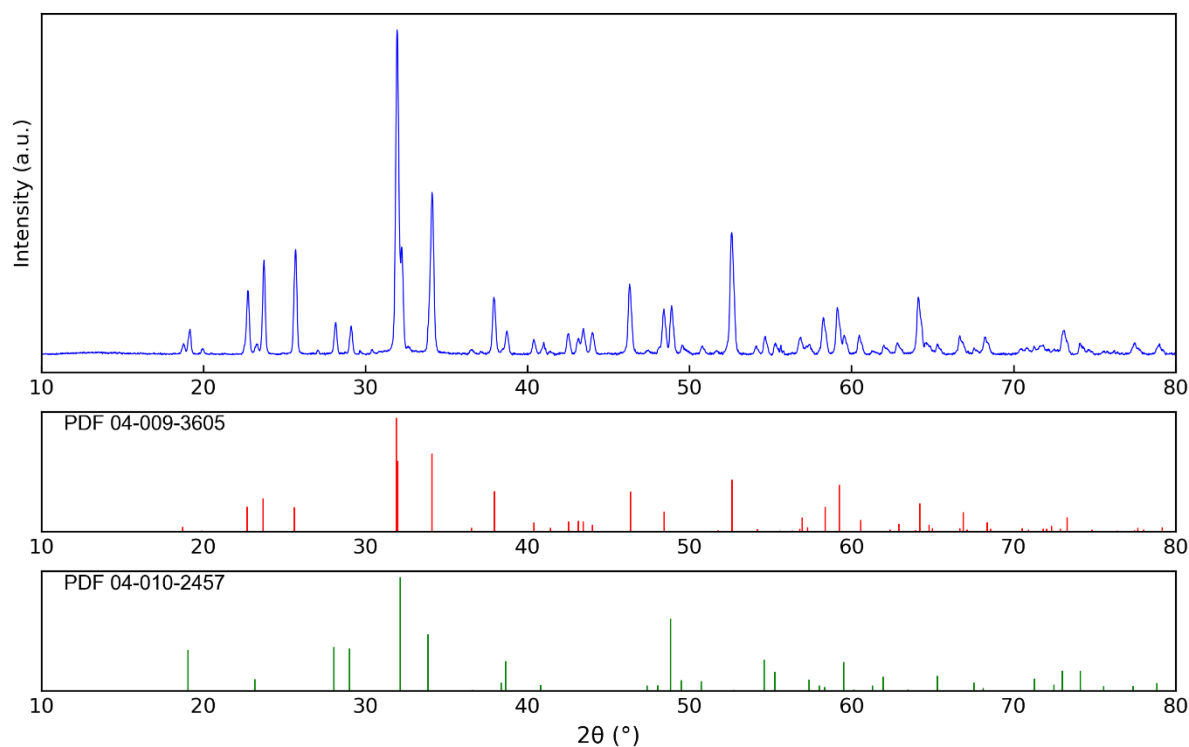

Figure A1. X-ray diffraction pattern of Na_2SO_4. Crystals were washed with ethanol and dried at T = 60°C, t>24h. Comparison is made with PDF 04-009-3605 (Sodium Sulfate) and PDF 04-010-2457(Sodium Sulfate, Thenardite, syn) for the same compound [126,127].

Appendix B

Feed composition

Table B1. Composition of the NMC 9.5.5 PLS before Mn removal. Uncertainties of three different measurements are reported. pH = 3.8 ± 0.1, E = 340 mV, I = 6.0 M.

	Co	Ni	Li	Mn	Na	SO_4^{2-}	P
C (g/L)	3.64 ± 0.04	44.1 ± 0.6	6.25 ± 0.08	1.72 ± 0.02	21.2 ± 0.25	55.1 ± 0.4	0.04 ± 0.00
C (mM)	62 ± 1	751 ± 10	900 ± 12	31 ± 1	923 ± 11	1719 ± 12	1.3 ± 0.1

Potentiometric Titration

To quantify the fraction of BTMPPA in the Cyanex 272, a potentiometric titration was performed following the procedure suggested in the technical brochure provided by Cytec (last update 19th June 2020). About 2.5g of Cyanex 272 were diluted in 50 mL of 75% v/v 2-propanol (≥99.8%, Sigma Aldrich, Germany) in distilled water and titrated against 0.1 N NaOH (Titrisol, Merck, Germany). An automatic titrator (Titrando 905, Metrohm, Switzerland) equipped with a pH probe (6.0257.600, Metrohm) and a 10 mL dosing unit (800 Dosino, Metrohm). The pH electrode was calibrated with pH buffers 2,4,7 and 10 (Merck). The experiment was performed in triplicates. Only one inflection point was observed, indicating that the quantity of 2,4,4-trimethylpentyl phosphonic acid in the system is below the LOQ of such technique. Using the second derivative method, a content of 91.3 ± 0.8 wt% (2.90 ± 0.01 M) of BTMPPA was computed.
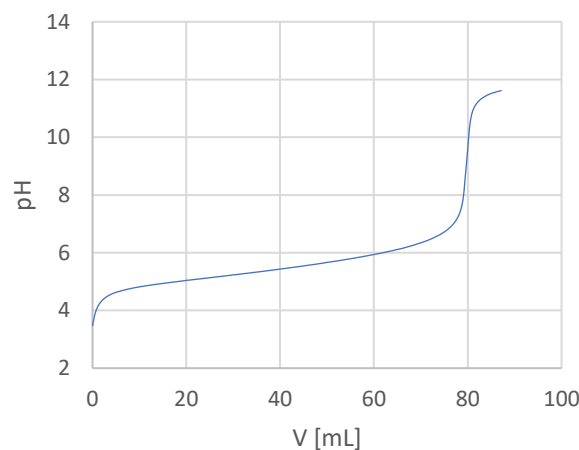

Figure B1. Potentiometric titration of Cyanex 272 in a mixture of 75% v/v 2-propanol and 25% v/v H_2O. [NaOH] = 0.1 M, T = 21 ± 1 °C. The curve for only one of the triplicates is reported for clarity (initial mass of Cyanex 272 = 2.5307 g).

ATR-FTIR 2φ*

The FTIR analysis of the upper and lower phases in the biphasic region named 2φ* for samples initially containing 33 wt% Cyanex 272 shows that in such a condition the system splits into a diluent rich (lighter) and diluent-depleted (heavier) phase. No viscosity measurements were carried out on the heavier phases, but it could be clearly observed that the viscosity increased with increasing NaOH concentration showing a gel-like consistence for the samples titrated with 5 and 10 M NaOH. Such behavior is most likely linked to the relative H_2O content of such phases, which decreases for higher NaOH concentrations.
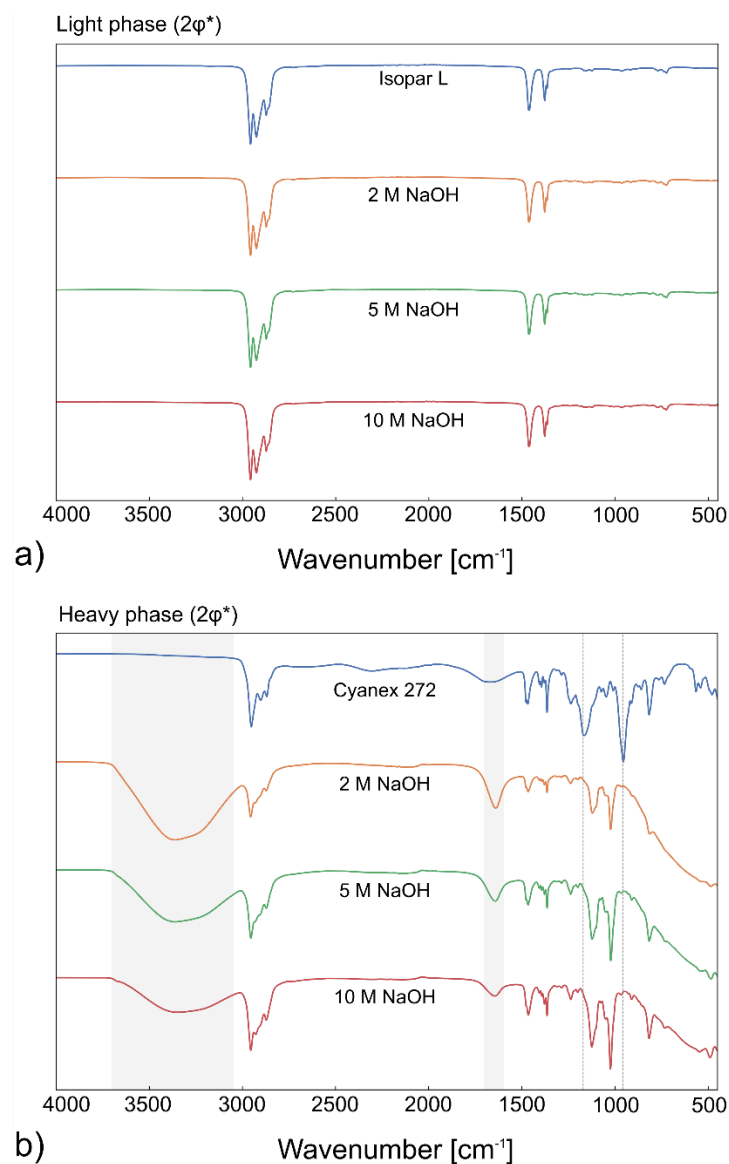

Figure B2. FTIR Spectra of light (a) and heavy (b) phases for 33 wt% Cyanex 272 in Isopar L 95% pre-neutralized with 2, 5 and 10 M NaOH. The composition of the system belongs to the biphasic region 2φ represented in the pseudo-ternary phase diagrams. The FTIR spectra of Isopar L and Cyanex 272 are reported as a reference.*

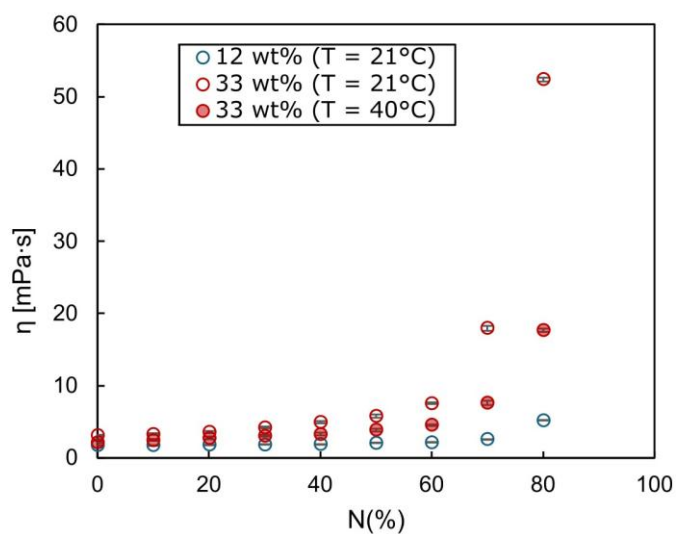**Viscosity as a function of the degree of saponification**

Figure B3. Viscosity of 12 and 33 wt% Cyanex 272 (0.3 M BTMPPA) in Isopar L as a function of the degree of pre-neutralization (N) at T = 21 and T = 40 ± 1 °C, [NaOH] = 10 M. The values reported for viscosity are an average over more than 10 shear rates in the range 0.63-100 s^{-1} and the uncertainty is <0.05 mPa·s in all cases. When the system was biphasic (N = 10, 20%), the viscosity of the upper (hydrophobic) layer was measured.